HHS Public Access

Author manuscript

J Colloid Interface Sci. Author manuscript; available in PMC 2022 May 15.

Published in final edited form as:

J Colloid Interface Sci. 2021 May 15; 590: 277–289. doi:10.1016/j.jcis.2021.01.047.

Nitric Oxide Releasing Halloysite Nanotubes for Biomedical Applications

Sama Ghalei[†], **Sean Hopkins**[†], **Megan Douglass**[†], **Mark Garren**[†], **Arnab Mondal**[†], **Hitesh Handa**[†,*]

[†]School of Chemical, Materials and Biomedical Engineering, University of Georgia, Athens 30602, United States

Abstract

Halloysite nanotubes (HNTs) are natural aluminosilicate clay that have been extensively explored for delivery of bioactive agents in biomedical applications because of their desirable features including unique hollow tubular structure, good biocompatibility, high mechanical strength, and extensive functionality. For the first time, in this work, functionalized HNTs are developed as a delivery platform for nitric oxide (NO), a gaseous molecule, known for its important roles in the regulation of various physiological processes. HNTs were first hydroxylated and modified with an aminosilane crosslinker, (3-aminopropyl) trimethoxysilane (APTMS), to enable the covalent attachment of a NO donor precursor, *N*-acetyl-*D*-penicillamine (NAP). HNT-NAP particles were then converted to NO-releasing *S*-nitroso-*N*-acetyl-penicillamine HNT-SNAP by nitrosation. The total NO loading on the resulting nanotubes was 0.101 ± 0.07 μmol/mg which could be released using different stimuli such as heat and light. Qualitative (Fourier-transform infrared spectroscopy and Nuclear magnetic resonance) and quantitative (Ninhydrin and Ellman) analyses were performed to confirm successful functionalization of HNTs at each step. Field emission scanning electron microscopy (FE-SEM) showed that the hollow tubular morphology of the HNTs was preserved after modification. HNT-SNAP showed concentration-dependent antibacterial effects against Gram-positive *Staphylococcus aureus (S. aureus)*, resulting in up to 99.6% killing efficiency at a concentration of 10 mg/mL as compared to the control. Moreover, no significant cytotoxicity toward 3T3 mouse fibroblast cells was observed at concentrations equal or below 2

[*]Corresponding Author: Hitesh Handa, School of Chemical, Materials, and Biomedical Engineering, University of Georgia, 220 Riverbend Road, Athens, GA 30605, Telephone: (706) 542-8109; hhanda@uga.edu.

Credit authorship contribution statement

Sama Ghalei: Conceptualization, Data curation, Formal analysis, Investigation, Methodology, Validation, Visualization, Writing - Original Draft, Writing - Review & Editing. **Sean Hopkins:** Investigation, Methodology, Validation, Writing – review and editing. **Megan Douglass:** Investigation, Validation, Writing – review and editing. **Mark Garren:** Investigation, Writing – review and editing. **Arnab Mondal:** Investigation, Writing – review and editing. **Hitesh Handa:** Resources, Funding acquisition, Project administration, Supervision, Writing – Review & Editing.

Conflict of Interest

The authors declare the following conflict of interest. Dr. Hitesh Handa is the founder of inNOveta Biomedical LLC which is involved in exploring possibilities of using nitric oxide releasing materials for medical applications.

Declaration of interests

The authors declare the following financial interests/personal relationships which may be considered as potential competing interests:

mg/mL of HNT-SNAP according to a WST-8-based cytotoxicity assay. The SNAP-functionalized HNTs represent a novel and efficient NO delivery system that holds the potential to be used, either alone or in combination with polymers for different biomedical applications.

Graphical Abstract

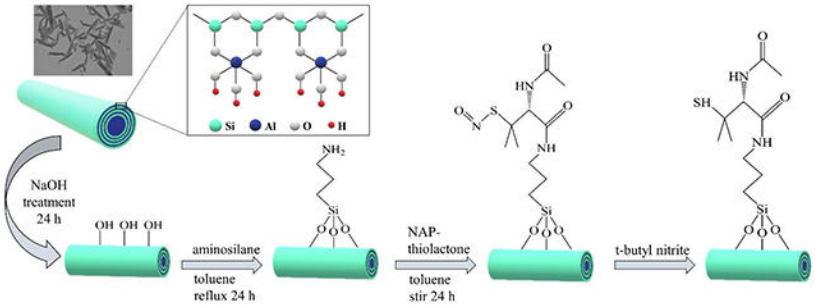

Keywords

nitric oxide; halloysite nanotubes; nanoparticles; S-nitroso-N-acetylpenicillamine; antibacterial; biocompatible; delivery system; biomedical application

1. Introduction

Nitric oxide (NO), a gaseous diatomic free radical produced endogenously, has been shown to possess a wide variety of physiological functions. The molecule was first identified as the endothelial-derived relaxing factor in the 1980s and its many other roles in biological processes were later discovered, such as cell proliferation, inhibition of platelet activation and adhesion, prevention of bacterial proliferation and biofilm formation, immune system regulation, angiogenesis, and wound healing [1, 2]. The wide-ranging and advantageous properties of NO in physiology have prompted many researchers to develop materials that can exogenously deliver NO for different biomedical applications [3, 4].

NO is generated *in vivo* by nitric oxide synthase (NOS) enzymes at the pico- to nanomolar range depending on the physiological function or site of generation. Therefore, the effective therapeutic dose of NO is determined by the final application. Regarding this, NO dose and release kinetics should be considered carefully in developing therapeutic NO delivery systems [5]. However, storage and precise spatiotemporal delivery of NO is technically challenging due to its short biological lifetime and high reactivity [6]. Owing to the difficulties of delivering NO gas directly, several types of NO donor molecules have been employed which can store and spontaneously release NO when placed under physiological conditions [7]. *S*-Nitrosothiols (RSNOs) in particular are an endogenous class of NO donor molecules and have received substantial attention for biomedical applications due to their versatility when being incorporated into polymeric medical devices. *S*-Nitroso-*N*-acetyl-penicillamine (SNAP), a synthetic tertiary RSNO derived from the amino acid penicillamine, has been utilized and studied extensively in combination with biomaterials due to its relatively high stability and nontoxic origins [8, 9].

Incorporating NO donors into biomaterials not only induces the desired therapeutic effects but also allows for localized control over NO release. In recent years, various NO-releasing biomaterials have been developed by either physical blending, solvent swelling, or covalently attaching NO donors into organic and inorganic formulations such as polymeric films, hydrogels, nanofibers, and micro/nanoparticles [10–14]. Despite having simpler production methods, physically blended or impregnating NO-releasing materials have issues with potential leaching of the donor molecules and by-products leading to decreased NO release lifetimes and potential cytotoxic effects. These issues can be circumvented by covalently linking the NO donor molecules to their underlying substrates, therefore increasing the stability and safety of NO-releasing scaffolds [15].

NO donors can be covalently attached to polymer backbones or submicron size inorganic filler particles [16–18]. Covalent attachment of NO donor molecules to the surface of filler particles has the advantage of imparting NO release properties to a wide range of biomedical polymers by simply blending the filler into the polymer. The mechanical properties of the polymeric substrate can be enhanced by the addition of these NO-releasing filler particles while simultaneously not affecting the polymer's backbone chemistry or crosslinking process. Moreover, by adjusting the amount of filler added and the type of polymer used, the NO release kinetics can be fine-tuned for specific applications [19]. A few numbers of research groups have previously reported the development of covalently attached NO donors (N,N-diazeniumdiolates and *S*-nitrosothiols) to filler particles such as porous and nonporous silica [20, 21], fumed silica nanoparticles [22, 23], and diatomaceous earth silica particles [24]. However, burst NO release kinetics and low attachment efficiency of NO donors to the modified surface of these particles mark two main factors limiting their efficacy. Therefore, seeking for novel NO carriers with improved storage and release properties remains an open challenge in the field of NO delivery.

For the first time in this study, covalent attachment of the *S*-nitrosothiol NO donor molecule, SNAP, to inorganic halloysite nanotubes (HNTs) is demonstrated. HNT [$Al_2(OH)_4Si_2O_5(2\text{-}H_2O)$] is a naturally occurring, biocompatible aluminosilicate clay with a hollow tubular structure. The tubular structure of halloysites is composed of silica on the outer surface and alumina at the innermost surface with an inner diameter of 10–30 nm, an outer diameter of 40–70 nm, and a length of 500–1500 nm [25]. The unique hollow nanotubular structure along with other attractive features such as high length-to-diameter ratio, availability in large amounts at low cost, mechanical strength, biocompatibility, and environmental friendliness, make HNTs highly suitable for a wide range of applications [26]. Applications of HNTs include various fields such as a carrier for the loading and controlled release of guest molecules, adsorbent for pollution remediation, personal care and cosmetics, template or nanoreactor for biocatalysis, and fabrication of polymer nanocomposites [27].

Specifically, the drug delivery potential of HNTs has received much attention in the biomedical field. Guest molecules can be either loaded into the inner lumen of HNTs or grafted onto the outer surface [28–31]. Different chemistry of the inner and outer surfaces in HNTs allows for separate modification and simultaneous immobilization of two or more active agents with different biological properties which offers an additional advantage over other nanofillers [32]. The successful loading of diverse active molecules such as

pharmaceuticals [33–35], biomacromolecules [36–39], corrosion inhibitors [40–44], and antibacterial agents [45–48] on HNTs has been previously demonstrated [49]. However, the delivery of NO gas using HNTs has never been explored.

In this work, the outer surface of HNTs was functionalized with the primary aminecontaining silane reagent, aminopropyltrimethoxysilane (APTMS). The terminal amine groups of APTMS modified HNTs were then reacted with NAP-thiolactone, a self-protected penicillamine derivative, yielding free sulfhydryl groups on the surface. After NAP attachment, the free sulfhydryl groups were nitrosated to form the corresponding SNAP derivatized HNTs. The efficiencies of both surface silylation and NAP-thiolactone attachment were evaluated. The chemical modification of HNTs and retention of nanotube morphology throughout the modification were confirmed by Fourier transform infrared spectroscopy (FTIR), Nuclear magnetic resonance (NMR), scanning electron microscopy (SEM), and transmission electron microscopy (TEM). Nitric oxide release over an 8 h period, total NO content, and storage stability at different conditions were determined by chemiluminescence. Finally, the antibacterial properties and cytocompatibility of the NO-releasing HNTs were examined.

2. Materials and methods

2.1 Materials

Halloysite nanotubes (HNTs) (quality level=100), *N*-Acetyl-*D*-penicillamine (NAP) (≥ 99.0% purity), (3-Aminopropyl) trimethoxysilane (APTMS) (97% purity), *L*-cysteine hydrochloride monohydrate (≥ 98.0% purity), Ellman's Reagent (5,5'-dithiobis(2-nitrobenzoic acid), DTNB) (≥ 98.0% purity), glycine hydrochloride (≥ 99.0% purity), 1,4,8,11-tetraazacyclotetradecane (cyclam) (≥ 98.0% purity), and *t*-butyl nitrite (≥ 96.0% purity) were purchased from Sigma-Aldrich (St. Louis, MO). Absolute ethanol (≥ 99.8% purity) was purchased from VWR (USA). Toluene (≥ 99.5% purity) and methanol (≥ 99.8% purity) were purchased from Fischer Scientific (Waltham, MA). Sodium acetate (≥ 99.9% purity) was obtained from EMD Chemicals, Inc. (Gibbstown, NJ). Luria-Bertani (LB) broth was obtained from Fisher Bioreagents (Fair Lawn, NJ). LB Agar was purchased from Difco Laboratories Inc. (Detroit, MI). Phosphatebuffered saline (PBS), pH 7.4, containing 138 mM NaCl, 2.7 mM KCl, and 10 mM sodium phosphate, was used for all *in vitro* experiments. Dulbecco's modified Eagle's medium (DMEM) and trypsin-EDTA were purchased from Corning (Manassas, VA 20109). The Cell Counting Kit-8 (CCK-8) was obtained from Sigma Aldrich (St. Louis, MO 63103). The antibiotic Penicillin-Streptomycin (Pen-Strep) and fetal bovine serum (FBS) were purchased from Gibco-Life Technologies (Grand Island, NY 14072). The bacterial strain *S. aureus* (ATCC 25922) and mouse 3T3 cells (ATCC 1658) were originally purchased from American Type Culture Collection (ATCC).

2.2 Preparation of *N*-Acetyl-*D*-penicillamine (NAP) thiolactone

Self-protected NAP-thiolactone was synthesized using the established protocol developed by Moynihan and Robert [50]. 5 g of NAP was dissolved in 10 mL of pyridine and a separate mixture of 10 mL of pyridine and 10 mL of acetic anhydride were also prepared. Both solutions were allowed to chill in an ice bath for 1 h before being combined and stirred at

room temperature for 24 h. The solution was then rotary evaporated at 60 °C to remove all the pyridine. The remaining viscous, orange crude was re-dissolved in chloroform and washed and extracted three times with 1M HCl. The organic layer was then dried using anhydrous magnesium sulfate and filtered. The chloroform was removed under vacuum at room temperature to obtain a solid product. The solid material was washed and filtered with hexane and allowed to dry overnight at room temperature before being stored at 4 °C.

2.3 SNAP functionalization of HNTs

2.3.1) HNTs purification and alkali treatment: HNTs were modified according to the previously reported literature with slight modification [51]. The as-received HNTs (3g) were purified with 30% H_2O_2 aqueous solution (10mL) and magnetically stirred for 2 h. The HNTs dispersion was then centrifuged and the resultant purified HNTs were first dried at 110 °C for 8 h in an oven and then dried at 60 °C in a vacuum oven for 4 h. To increase the number of hydroxyl groups on the surface, HNTs were treated with sodium hydroxide (NaOH). 2 g of HNTs were dispersed into 100 mL of 0.01 M NaOH solution and sonicated for 10 min using a water bath sonicator (Ultrasonic cleaner, Branson 2800) to obtain a homogeneous dispersion and magnetically stirred for 24 h at room temperature. The resultant hydroxylated HNTs (HNT-OH) were collected by centrifugation and rinsed several times with water until the pH reached near neutral. The prepared HNT-OH were dried at 110 °C for 8 h then at 60 °C for 4 h under vacuum.

2.3.2) Surface silylation: Surface silylation of HNTs was carried out following the previously reported literature with slight modification [52]. 0.3 g of hydroxylated HNTs were added to 10 mL of dry toluene and sonicated for 10 min to obtain a uniform dispersion. 1 mL of (3-aminopropyl) trimethoxysilane (APTMS) was added and the solution was refluxed under constant stirring for 20 h at 120 °C. The product was recovered by centrifugation and washed with toluene several times to remove the excess organosilane. APTMS modified HNTs (HNT-APTMS) were dried under vacuum at 60 °C for 24 h.

2.3.3) NAP-thiolactone attachment and nitrosation: The silanized HNTs were further reacted with NAP by slightly modifying a protocol by Frost et al [22]. Equal amounts (0.2 g) of HNT-APTMS and NAP were suspended in 15 mL toluene and allowed to stir for 24 h at room temperature to obtain NAP derivatized HNTs (HNT-NAP). Nitrosation of the formed HNT-NAP was done by adding *t*-butyl nitrite. *T*-butyl nitrite was first chelated of any copper contaminants by vortexing it with an equal volume amount of 20 mM cyclam solution and repeated three times. The organic *t*-butyl nitrite layer was then separated into an amber vial and stored at 5 °C. 500 μL of *t*-butyl nitrite was then added to 15 mL of HNT-NAP to form a green, HNT-SNAP dispersion. The nitrosated nanotubes (HNT-SNAP) were then collected by centrifugation, washed several times with fresh toluene, vacuum-dried at room temperature, and stored in the dark at 4 °C.

2.4 Ninhydrin primary amine quantification

The amount of amine groups bound to the surface of HNT-APTMS was estimated by using the ninhydrin assay. 2 mL of HNT-APTMS dispersions in 0.05% glacial acetic acid was combined with 1 mL of ninhydrin reagent and the mixture heated in a boiling water bath for

10 min. After cooling to room temperature, the samples were brought to a total volume of 8 mL with 95% ethanol and the absorbance was measured at 570 nm using a UV–vis spectrophotometer (Thermo Scientific Genesys 10S UV–vis). The amine content of HNT-APTMS samples was quantified using a calibration curve of known glycine hydrochloride concentrations.

2.5 Ellman's test for free sulfhydryls

Ellman's Reagent, DTNB (5,50-dithio-bis-[2-nitrobenzoic acid]), was used to determine the amount of thiol groups on the surface of HNT-NAP nanotubes. Briefly, a stock DTNB solution containing 2 mM DTNB and 50 mM NaAc was prepared and used to create a working DTNB solution consisting of 50 μL of DTNB stock solution, 100 μL of PBS, 800 μL of H20, and 50 μL of the sample. Absorbance values for each sample were recorded with a UV–vis spectrophotometer (Thermo Scientific Genesys 10S UV–vis) at a wavelength of 412 nm. The number of thiol groups was calculated from a standard curve of L-cysteine at pre-known concentrations.

2.6 Fourier-transform infrared spectroscopy (FTIR) and Nuclear Magnetic Resonance (NMR)

The successful functionalization of HNTs at each step was analyzed using Fourier transform infrared spectroscopy (FTIR). The HNT powders before and after modification were formed into a disk after mixing with potassium bromide (KBr) with a ratio of 1:100. For each measurement, the spectra were obtained from 128 scans with a resolution of 4 cm^{-1} over the wavenumber range of 400–4000 cm^{-1}.

Solid-state cross-polarization magic angle spinning carbon-13 nuclear magnetic resonance (CP/MAS ^{13}C NMR) was performed using a Bruker NEO 600 MHz spectrometer equipped with a 4mm rotor CMP-HRMAS probe. Due to the low carbon count with respect to the HNT element composition, final NMR spectra were obtained from the summation of 18 spectra at 256 scans at a spinning speed of 10 kHz. Carbons were detected and characterized on both the APTMS and NAP modified HNTs.

2.7 Nitric oxide release and storage stability measurements

NO release from HNT-SNAP was measured via chemiluminescence using a Sievers nitric oxide analyzer (NOA) model 280i (Boulder, CO). Samples were weighed and incubated in 0.01 M PBS containing EDTA at 37 °C in an amber reaction vessel to protect from light. Nitric oxide released from the suspension of nanotubes was continuously swept from the vessel by an N_2 purge gas at a flow rate of 200 mL min^{-1} into the NOA system. The NO levels in the ppb unit measured at each time point were converted to NO release rate in mol min^{-1} mg^{-1} using the NOA instrument constant, determined by quantitative reduction of a known amount of nitrite. Between the final and initial NOA measurements, the samples were stored in 0.01 M PBS with EDTA at 37 °C. NO release at different temperatures was measured by placing the sample vial in 4 °C, room temperature (RT), 37 °C, and 45 °C water bath, respectively. Using the same instrument, light-triggered NO release from HNT-SNAP was also measured by placing the nanotubes in clear sample vials and irradiating them with a light-emitting diode (LED) lamp (12 W).

To measure the total NO loading, alternating injections of 0.25 M copper (II) chloride and ascorbic acid were added to the NOA reaction vessel. These injections catalytically triggered the release of all NO present in the sample within a time frame measurable by NOA. The total amount of NO released was calculated by the integration of NO release rate curves. Storage stability of the HNT-SNAP was examined by storing the samples under light and dark conditions at ambient temperature and in the freezer (−20 °C). After 4 weeks, the NO content in each sample was measured and compared to the initial total NO loading to calculate the % NO remaining.

2.8 Morphology observation

The morphology of the nanotubes was observed by field emission scanning electron microscopy (FE-SEM). Transmission electron microscopy (TEM) images were used to measure the size of nanotubes before and after modification. Dilute HNT dispersions in DI water were dropped onto a carbon-film supported Cu grid and dried. Then the samples were observed using a JEOL JEM-2100 transmission electron microscope under an accelerating voltage of 200 kV. In order to compare the diameter of different HNT samples, ImageJ software was used to measure the widths of 50 tubes from the TEM images.

2.9 *In vitro* antibacterial assay

To assess the antibacterial activity of the derivatized halloysite nanotubes, a 24 h antibacterial assay was performed against *S. aureus* (ATCC 6538) based on a previously established protocol [53]. Bacteria were handled in a BSL-2 facility previously approved by the University of Georgia. An isolated strain of *S. aureus* was inoculated in LB broth at 150 rpm at 37 °C. After 16 h, the bacterial solution was centrifuged at 2500 rpm for 7.5 min and washed with sterilized PBS (pH 7.4). The solution was again centrifuged at 2500 rpm for 7.5 min and resuspended in sterilized PBS through vortexing. The bacterial solution was diluted with PBS to reach a concentration of ~10^7 colony-forming units (CFUs) per mL. Using a 96-well plate, 100 μL of the bacterial solution was plated with 100 μL of HNT (concentrations ranging from 0.5 mg/mL–10 mg/mL) suspended in PBS (n=5). Wells absent of nanotubes were used as control. The plate was incubated at 37 °C at 150 rpm for 24 h. After incubation, solutions in each well were serially diluted and plated on LB agar plates. Plates were incubated overnight at 37 °C. After incubation, CFUs present on the plates were counted to determine the effect of the presence and concentration of control and NO-releasing halloysite nanotubes on the viability of *S. aureus*, which represent the number of viable CFUs present per mL. The % reduction in bacterial viability was calculated according to the following equation (C = CFUs per mL):

$$Reduction\ of\ bacterial\ viability\ (\%) = \frac{C_{control} - C_{sample}}{C_{control}} \times 100 \quad \text{(Eq. 1)}$$

2.10 Cell culture and viability studies

3T3 mouse fibroblast cells (ATCC 1658) were cultured in a 75 cm^2 T-flask containing complete DMEM medium with 10 % fetal bovine serum (FBS) and 1 % penicillin–streptomycin to prevent contamination. The T-flask with cells was incubated at 37 °C, in a 5

% CO_2 humidified environment to allow for monolayer formation. The culture medium was changed every two days, and cells were checked daily for growth and contamination. After the confluency reached above 80 %, cells were trypsinized (0.18 % trypsin and 5 mM EDTA) and detached from the T-flask. Finally, the cells were counted under a hemocytometer using Trypan blue (dye exclusion method). The effect of modified HNTs on cell viability was determined by the CCK-8 cell counting kit according to the manufacture's protocol (Sigma Aldrich). The CCK-8 test is nondestructive in nature and more sensitive than other tetrazolium salts such as MTT, XTT, WST-1, and MTS. The number of living cells is directly proportional to the amount of formazan dye (orange color) generated by the interaction of the highly water-soluble tetrazolium salt, WST-8, with dehydrogenases in the cells and is detected at the absorbance maxima of 450 nm. First, cells were seeded in 96-well plates at a density of 5000 cells per well and allowed to attach in a humidified incubator with 5 % CO_2 for 24 h. The media were then replaced with fresh media containing unmodified HNTs or HNT-SNAP at various concentrations (0.5 mg/mL-10 mg/mL) and incubated for another 24 h. Cells maintained in DMEM without HNTs were used as a control group. To avoid absorbance interference by HNTs and HNT-SNAP, the media containing nanotubes was removed and 100 μL fresh media plus 10 μL of CCK-8 solution was added into each well and incubated for an additional 2 h at 37 °C. The absorbance was detected at 450 nm. The data were expressed as mean ± standard deviation (SD) (n=6), and the cell viability was calculated using the following equation [54]:

$$Cell\ viability\ (\%) = \frac{Absorbance\ (treated\ cells)}{Absorbance\ (control\ cells)} \times 100 \quad \text{(Eq. 2)}$$

2.11 Statistical Analysis

All data are reported as a mean ± standard deviation collected from three data points unless otherwise noted. A one-way analysis of variance was used to compare any significant differences. p-values of < 0.05 were considered statistically significant.

3. Results and discussion

3.1 Chemical Synthesis

Fig. 1 shows a schematic representation of HNT functionalization with SNAP. HNTs are first treated with NaOH to create hydroxyl groups on their external surface. It is previously reported that NaOH can effectively react with the tetrahedral silicate to create silanol (SiOH) groups [51, 55]. After base treatment, HNTs are functionalized with aminopropyltrimethoxysilane (APTMS) by a silane coupling reaction. Silanization reactions proceed via a two-step process: (i) hydrolyzation of silanol groups in presence of water and (ii) condensation of silanol groups with SiOH groups present on the HNT-OH surface [56]. APTMS is a reactive aminosilane coupling agent that is widely used to modify the surface of HNTs [57, 58]. APTMS consists of three methoxy moieties that allow for stable surface binding and the formation of an amine rich layer on the surface. Afterward, NAP-thiolactone, a self-protected penicillamine derivative, is anchored to the amine groups by a ring-opening reaction resulting in a tertiary thiol-bearing silane. The thiol groups are then

readily converted to their corresponding *S*-nitrosothiols by reaction with *t*-butylnitrite. The nitrosated nanotubes are referred to as HNT-SNAP.

3.2 FTIR and NMR

The surface modification of HNT by NaOH and further chemical functionalization by APTMS and SNAP were confirmed by FTIR analysis. Fig. 2 shows the FTIR spectra of HNT, HNT-OH, HNT-APTMS, and HNT-NAP. In the unmodified HNT spectrum, the peaks at 3700 cm^{-1} and 3620 cm^{-1} are assigned to the stretching vibrations of hydroxyl groups on the external and internal surface of HNT. The vibration at 1640 cm^{-1} corresponds to O-H deformation of water and bands at 1030 cm^{-1} and 910 cm^{-1} exhibit the asymmetrical Si-O-Si stretching and Al-OH bending vibrations, respectively. The intensity of Si-O-Si stretching peak at 1030 cm^{-1} is increased in the HNT-OH FTIR spectrum compared to the unmodified HNT. This indicates the formation of SiOH groups on the surface of HNTs according to a previous study [59]. After functionalization of HNT-OH by APTMS (HNT-APTMS), new characteristic peaks appeared at 2940 cm^{-1}, 1554 cm^{-1}, and 1490 cm^{-1} which are respectively attributed to C-H stretching vibrations of alkyl groups, bending vibrations of NH_2, and antisymmetric stretching vibrations of C-N in APTMS. Moreover, the OH stretching band at 3620 cm^{-1} is widened which might be due to the overlap of OH with the NH_2 stretching vibrations signal around 3360 cm^{-1}. These results indicate that APTMS has been successfully grafted onto HNT. The covalent attachment of NAP-thiolactone on HNT-APTMS was shown by characteristic peaks for amide conjugation in the respective FTIR spectrum. The new absorption band observed at 1657 cm^{-1} denotes carbonyl vibrations and the signal at 1540 cm^{-1} is ascribed to N-H bending vibrations. Additionally, the sp^3 C-H bonds consistent with the alkyl chain of APTMS and methyl groups in NAP are also seen in subtle vibrations at 3051 cm^{-1} and 2916 cm^{-1}. Further analysis of the surface modifications of the HNTs was done through CP/MAS ^{13}C NMR. Fig. 3 shows the modification of APTMS to the HNTs and the subsequent attachment of NAP. The carbon peaks that form on the HNT-APTMS are identical to the ppm shifts seen from a previous study which attached a similar aminopropyl silane molecule to HNTs [60]. Signals observed at 42.58, 25.76, and 10.00 ppm match with the three carbons present on the APTMS. After the attachment of NAP, a characteristic carbonyl peak at 171.00 ppm is seen, proving there was a successful ring-opening reductive amination reaction. While some of the carbons were difficult to differentiate in the methyl region (between 15–30 ppm) due to overlapping signals, there was an overall increase in total carbons after integrating the region when compared to the HNT-APTMS spectrum. Therefore, these results strongly suggest that NAP-thiolactone is covalently attached to the HNT-APTMS.

3.3 Quantitative characterization of functionalized HNTs

To quantify HNT surface modifications and measure overall reaction efficiencies, the primary amine content, the resulting sulfhydryl content, and the total NO loading of HNTs after reaction with *t*-butyl nitrite were assessed (Table 1).

3.3.1) Primary amine content: Ninhydrin assay was performed to measure the primary amine groups of aminosilanes grafted on the surface of HNT. Ninhydrin reagent reacts with primary amines via oxidative-reductive reactions to generate a colored product known as

Ruhemann's purple. The absorbance of the Ruhemann's complex at 570 nm is proportional to the surface amine density [61]. The amount of amine groups on the surface of HNT was estimated to be 0.252 ± 0.009 μmol/mg. Prior measurement, HNT-APTMS were thoroughly washed to eliminate the nonsurface bound silanes. Therefore, the measured amine content is attributed to covalent aminosilanes grafting and not to physical surface adsorption.

3.3.2) Sulfhydryl content: It is previously reported that NAP-thiolactone exposes its thiol group only upon the ring-opening reaction with amine functional groups [62]. Therefore, the amount of NAP-thiolactone covalently attached to HNT-APTMS can be determined by measuring the number of primary thiols. The free thiol concentration on modified HNT's surface after NAP-thiolactone attachment was determined by means of Ellman's assay. Ellman's reagent, 5,5'-dithiobis-(2-nitrobenzoic acid) (DTNB) reacts with the thiol functional group to form a mixed disulfide and dianion of 2-nitro-5- thiobenzoic acid (TNB^{2-}) in water. This solution has a distinctive yellow color that can be quantified by measuring the absorbance of visible light at 412 nm [63]. Using this method, the free sulfhydryl content of HNT-NAP was found to be 0.202 ± 0.015 μmol/mg indicating a NAP-thiolactone attachment efficiency (conversion ratio) of 80%. The conversion ratio obtained in this study is significantly higher than what was previously reported in the literature (~ 2.5-47 %) for covalent attachment of NAP-thiolactone to aminosilane modified silica-based particles [22, 24, 64]. According to the previous studies, low values of conversion ratios are usually associated with aminosilanes self-polymerization and the formation of highly dense, interconnected silane networks causing steric congestion for NAP-thiolactone ring-opening reaction. However, in this study moderate reaction temperature, low silane concentration, and multiple washings with organic solvents advantageously minimize the formation of aminosilane-based oligomers and polymers.

3.3.3) Total NO loading: The total NO loading of HNT-SNAP was monitored via NOA using multiple injections of 0.25 M copper (II) chloride and ascorbic acid to trigger complete NO release. HNT-SNAP could store up to 0.101 ± 0.07 μmol/mg NO after nitrosation with *t*-butylnitrite demonstrating a nitrosation efficiency of ~50%. According to the previous studies, the incomplete nitrosation of HNT-SNAP is most likely caused by thiols that exist as disulfides or that are inaccessible to the nitrosating agent due to the associated steric hindrance surrounding the tertiary thiol functionality [64, 65]. Nevertheless, the total NO loading of HNTs is about three orders of magnitude larger than the previously reported SNAP functionalized diatomaceous earth silica particles and is almost equal to the total NO loading of SNAP grafted fumed silica particles [22, 24]. The obtained results after quantification of primary amines, thiol groups, and total NO content of modified HNTs along with the calculated reaction efficiencies are summarized in Table 1.

3.4 *In vitro* release kinetics of HNT-SNAP

NO release from *S*-nitrosothiols (RSNOs) such as SNAP can easily occur by cleavage of the S–NO bond in presence of either heat, light, or certain metal ions leading to the formation of free NO and disulfide species (RSSR) (Eq. 3) [8]. NO release from HNT-SNAP was studied under different stimuli including light and various temperatures.

$$2RSNO \rightarrow RSSR + 2NO \quad \text{(Eq. 3)}$$

The main mechanism of NO release from *in vivo* administered NO delivery systems is the thermal decomposition of SNAP via heat and moisture. Therefore, NO release measurement was first carried out at 37 °C in dark. Fig. 4 shows both the real-time and cumulative NO release from HNT-SNAP at different time points over the course of 8 h. The cumulative percentage was obtained by integrating the real-time NO release rates with the trapezoidal rule and dividing it by the total amount of NO initially loaded onto HNT-SNAP. The instantaneous release profile showed an initial rapid NO release over the first two hours followed by a slower release rate for 8 h. The burst effect during the first hours may correspond to the loosely bound aminosilane-SNAP complexes trapped within HNTs or less entangled SNAP functional groups that are exposed to the matrix environment. The cumulative release of NO within 8 h reached up to 47.4 ± 3.9% meaning that the release half-life of HNT-SNAP is more than 8 h. This indicates a remarkable improvement upon the release kinetics of previously reported NO-releasing silica nanoparticles that reportedly deliver more than half of their NO payload in less than 2 hours [20, 22, 23, 66]. Covalent attachment of SNAP to HNT results in a total NO release of 0.101 ± 0.07 μmol/mg for over 8 h and may also decrease unwanted side effects and toxicity caused by leaching of the donor or reaction by-products commonly caused by physically blending them within a polymer.

The light-induced NO release from HNT-SNAP was also tested by irradiating the nanotubes with a white LED light (12 W) and is shown in Fig. 5. HNT-SNAP released NO at a constant rate of ~7 ppb/mg when the light was off. However, by switching the light on, a significant increase in the NO flux was observed resulting in a sharp peak in the NO release profile (Fig. 5). This process was repeated three times and the peak intensities were decreased in time as the NO reservoir was drawn down. The light-triggered NO release properties of SNAP and *S*-nitrosoglutathione (GSNO) NO donors doped within polydimethylsiloxane films have been previously studied using an LED light source with different wavelengths [67].

In addition to light, the effect of temperature on NO release kinetics of HNT-SNAP was studied and the results are presented in Fig. 6. HNT-SNAP showed a very low amount of NO release at 4 °C with an average rate of 3 ppb/mg. A higher NO flux of about 7 ppb/mg was obtained at room temperature which was further increased to 31 ppb/mg and 50 ppb/mg by elevating the temperature to 37 °C and 45 °C, respectively. By lowering the temperature back to RT, the NO flux was shortly decreased down to about 7 ppb/mg again. Overall, these results demonstrate the ability of HNT-SNAP to release tunable amount of NO by using light and adjusting the temperature which can prove useful for versatile biomedical applications.

The kinetics of NO release from HNT can be further modulated by incorporating these inorganic fillers into polymeric substrates to limit the exposure of SNAP molecules to the media and prevent a rapid release. The fluxes of NO can be finely tuned depending upon the application by changing the polymeric matrix (and the associated water uptake properties) or

altering the amount of HNT-SNAP blended into the polymer. Additionally, certain metal ions (e.g. Cu^{+}) that are shown to have a catalytic effect on the release of NO from *S*-nitrosothiols can be loaded on the outer walls or into the inner lumen of HNTs to enhance NO release [53, 68–71]. In fact, using this approach allows for obtaining different NO release profiles for versatile biomedical applications such as platelet inhibition, bacteria-killing, and wound healing.

The stability of HNT-SNAP was evaluated by measuring the NO content after storing them at different conditions (light at room temperature, dark at room temperature, and −20 °C freezer) for a period of 4 weeks. HNT-SNAP showed the highest stability in the freezer with 97.2 ± 2.7 % of NO being remained after storing at −20 °C for 4 weeks (Fig. 7). While the lowest stability was attributed to HNT-SNAP stored under light at room temperature (RT) with only 53.8 ± 3.2 % of NO being remained after 4 weeks. As expected, HNT-SNAP stored at dark in RT could preserve a significantly higher amount of NO (67.3 ± 4.5 %) compared to HNT-SNAP stored under light at the same temperature.

3.5 Morphological Analysis

The TEM and FESEM images of unmodified HNT and HNT-SNAP are depicted in Fig. 8. Both FESEM and TEM images display the polydispersity and hollow tubular structure of nanotubes with an open-ended lumen along the tube. From TEM images, the size of HNTs was measured to be 100–1000 nm long, with an outer diameter of about 60 nm and a lumen diameter of about 10 nm. After modification with SNAP, the outer walls of HNTs became slightly thicker (~70 nm), indicating that the functionalization is occurring on the outer surface of nanotubes [72].

In addition to size, the morphology of nanomaterials is also a critical factor affecting their loading capacity and release kinetics. For instance, NO-releasing fumed silica particles have been previously developed and studied for biomedical applications. However, aggregation of these particles into coarse, irregular clusters upon pyrolytic production, renders their final morphology and NO release kinetics highly unpredictable [73]. In contrast, HNTs are well known for their excellent dispersion ability originating from their stable tubular morphology, charge distribution, and unique crystal structure [74]. To obtain reliable and consistent NO release kinetics, it is imperative to maintain the original morphology of HNTs after chemical modifications. Apart from loading and controlled release of guest molecules, morphological properties of HNTs can also significantly affect their performance in other applications such as the fabrication of HNT-polymer nanocomposites, nanoreactor templates, and filtration purposes [75]. As can be seen in the FESEM and TEM images, the tubular morphology and crystal structure of HNTs are preserved after chemical modifications with APTMS and SNAP. While the original tubular morphology of the HNTs is preserved, the SEM images seen in Fig. 8 also demonstrate a rougher surface interface on the HNT-SNAP when compared to control HNTs. This is most likely due to a hydrolysis reaction between APTMS chains, creating a polymerized siloxane layer at the HNT interface. Since the reaction conditions mentioned previously were not perfectly anhydrous, this type of hydrolysis is commonly seen [76].

3.6 Bactericidal properties of HNT-SNAP

Over the past few years, increasing attention has been focused on nanoparticle-based materials in the field of antimicrobial therapies. Administration of antimicrobial agents using nanoparticles provide several benefits over free antimicrobial agents such as improved solubility, pharmacokinetics, and therapeutic index of the drug, reduced side effects, as well as controlled release and targeted delivery of the drug to the site of infection [77, 78]. One of the most common causes of hospital-acquired infections is the gram-positive *S. aureus* bacteria [79]. Currently, successful treatment of infections caused by *S. aureus* is being restricted as this microorganism has developed resistance toward silver and many antibiotics [80, 81]. Therefore, alternative therapeutic approaches are essentially needed. Nitric oxide is known to be a potent antimicrobial agent that kills bacteria through rapid and nonspecific mechanisms [82]. Therefore, the incidence of bacterial resistance is minimized as opposed to antibiotics and silver nanoparticles. According to the literature, chemical alteration of DNA, disturbing protein synthesis, damaging cell membrane amino acids, and lipid peroxidation are the main bactericidal mechanisms of nitric oxide [83]. In this study, the antibacterial activity of HNT and HNT-SNAP toward *S. aureus* was studied as a proof-of-concept evaluation for biomedical applications. The result of bacterial viability was quantified using a CFU counting methodology and is depicted in Fig. 9. The reduction efficiency values of all the tested concentrations of HNT-SNAP are also presented in Table 2. HNT-SNAP showed antibacterial activity against *S. aureus* in a concentration-dependent manner. By increasing the HNT-SNAP concentration from 0.5 mg/mL to 10 mg/mL, the bacteria reduction efficiency was enhanced from 48.9% to 99.6% (> 2 log reduction), whereas, unmodified HNT showed no antibacterial activity against *S. aureus* regardless of the concentration, suggesting that the antibacterial activity of HNT-SNAP is attributed solely to the NO release. Additionally, it has been previously shown that NO donors either physically blended or covalently attached to biomaterials exhibit antibacterial effects toward different bacteria including *P. aeruginosa, S. aureus, and E. coli* [84, 85]. The previously demonstrated antibacterial properties of NO against these bacteria along with the antibacterial effects of HNT-SNAP displayed in this study provide promising perspectives for the potential application of HNT-SNAP either alone or in combination with other biomaterials. Moreover, this work marks a significant improvement upon the antibacterial properties of previously reported NO-releasing diatomaceous earth (DE) silica particles by our group [24]. HNT-SNAP at concentrations of 5 mg/mL and 10 mg/mL reduced the number of *S. aureus* bacteria by 94.4 ± 1.9 % and 99.6 ± 0.1 % respectively, whereas a lower reduction efficiency of 92.9 ± 2.6 % was reported for SNAP modified DE silica particles at an even greater concentration of 21.5 mg/mL. The superior bactericidal efficiency of HNT-SNAP might be the result of enhanced total NO loading and higher flux of NO release. According to a study by Nichols and Schoenfisch, the bactericidal properties of NO-releasing surfaces are dependent on the NO payload, rate of delivery, and duration of NO release [86].

3.7 Cytocompatibility of HNT-SNAP

While we were able to demonstrate a significant reduction in bacterial viability due to the NO release of the HNT-SNAP, it is imperative that they exhibit no toxic effects towards mammalian cells. To assess the cytotoxicity of HNT-SNAP, the direct contact CCK-8

(Sigma-Aldrich) method was performed on mouse fibroblast cells (ATCC). Cells were exposed to different concentrations of nanotubes ranging from 0.5 mg/mL to 10 mg/mL. The results of the test are depicted in Fig. 10 and cell viability values for HNT and HNT-SNAP at all the tested concentrations are reported in Table 3. No significant cytotoxicity was observed for both unmodified HNT and HNT-SNAP at concentrations below 2 mg/mL as compared to control (wells without any nanotubes). However, by further increasing the concentration of nanotubes to higher values (≥ 2 mg/mL), the number of viable cells decreased and reached less than 50% of the control at 10 mg/mL (p-value < 0.05). It is noteworthy to mention that, at all concentrations, the viability of cells exposed to HNT-SNAP remained higher than the cells treated with unmodified HNT. The higher viability of cells in contact with HNT-SNAP can be explained by the previously described regulating effects of NO on fibroblasts proliferation. In the past, several reports have demonstrated that exogenously applied NO, at low concentrations, is able to increase the growth and proliferation of several mammalian cell lines including fibroblasts [87–89]. The *in vitro* and *in vivo* cytotoxicity of HNT have also been extensively studied and described by many research groups, all in agreement that HNT shows a high level of cytocompatibility and low cytotoxicity [49]. Therefore, the reduction in the viability of cells at higher concentrations of HNT-SNAP is most likely attributed to the high number of particles. Despite the development of many nanoparticulate NO delivery systems, only a few studies have investigated the cytocompatibility of these nanosized delivery systems in direct contact with cells. We have previously shown that regardless of the biocompatibility of the substrate and the loaded NO donor, NO-releasing nanoparticles at high concentrations (5–10 mg/mL) can induce toxicity toward fibroblast cells [90]. However, this toxic effect was found to be solely related to the high number of nanoparticles covering the cells in the well plate. Similar results have also been reported by Nurhasni et al., evaluating the cytotoxicity of NO-releasing poly(lactic-co-glycolic acid)-polyethyleneimine nanoparticles against mouse fibroblast cells [91]. Collectively, our results demonstrate that SNAP functionalized HNTs show tunable NO release, strong antibacterial properties, and desirable cytocompatibility which may prove useful for a range of applications. To further confirm the preclinical potential of HNT-SNAP, comprehensive *in vivo* verification of the *in vitro* results is required.

4. Conclusion

Covalent attachment of the nitric oxide (NO) donor molecules to inorganic filler particles is an effective approach to impart NO release properties to a wide range of biomedical polymers and enhance their safety and stability by reducing the potential leaching of the donor molecules and by-products. However, burst NO release kinetics and low attachment efficiency of NO donors to the modified surface of these particles mark two main factors limiting their efficacy. With the goal of improving these properties, this paper aimed to develop and characterize a novel NO delivery system based on halloysite nanotubes (HNTs). (3-aminopropyl) trimethoxysilane (APTMS) functionalization of HNT facilitated the covalent attachment of *N*-acetyl-*D*-penicillamine (NAP) which was further converted to *S*-nitroso-*N*-acety1-penicillamine (SNAP), the NO donor molecule. The amount of primary amine groups after APTMS modification and thiol groups after NAP attachment were

estimated to be 0.252 ± 0.009 μmol/mg and 0.202 ± 0.015 μmol/mg respectively, indicating a favorably high conversion ratio of 80%. In total, each mg of HNTs was loaded with 0.101 ± 0.07 μmol of NO which were released sustainably over an 8 h period. The high conversion ratio and NO release half-life of more than 8 h obtained for HNT-SNAP demonstrated a significant improvement upon the previously reported NO-releasing silica particles [20–24]. Light-triggered NO release from HNT-SNAP was also studied using a light-emitting diode source and it was found that NO fluxes were notably increased immediately upon irradiation. The release of NO from HNT-SNAP could also be fine-tuned by adjusting the temperature. The successful modification of HNT was further confirmed and studied using Fourier transform infrared spectroscopy and ^{13}C Nuclear magnetic resonance. The field emission scanning electron microscopy (FE-SEM) images showed that the unique morphology of HNTs remains intact throughout the synthesis. However, according to transmission electron microscopy (TEM) images, the outer walls of HNTs became slightly thicker after surface modification. Additionally, the bactericidal efficiency of HNT-SNAP towards gram-positive *S. aureus* and biocompatibility with mammalian cells were demonstrated at different concentrations ranging from 0.5 mg/mL to 10 mg/mL. Based on the promising results obtained in this study and the myriad of potential applications of NO-releasing materials, it can be concluded that modification of HNTs with NO donor molecules open up the use of these nanomaterials for several applications in the biomedicine field such as implants, catheters, tissue engineering scaffolds, wound dressings, biosensors, and medical device coatings. The results of this study form the basis for further future studies in the pre-clinical settings to ascertain the therapeutic potential of NO-releasing HNTs.

Acknowledgments

Funding for this work was supported by the National Institutes of Health, USA grant R01HL134899.

References

[1]. Loscalzo J, The identification of nitric oxide as endothelium-derived relaxing factor, Circ Res 113(2) (2013) 100–3. [PubMed: 23833290]

[2]. Wo Y, Brisbois EJ, Bartlett RH, Meyerhoff ME, Recent advances in thromboresistant and antimicrobial polymers for biomedical applications: just say yes to nitric oxide (NO), Biomater Sci 4(8) (2016) 1161–83. [PubMed: 27226170]

[3]. Jen MC, Serrano MC, van Lith R, Ameer GA, Polymer-Based Nitric Oxide Therapies: Recent Insights for Biomedical Applications, Adv Funct Mater 22(2) (2012) 239–260. [PubMed: 25067935]

[4]. Seabra AB, Durán N, Nitric oxide-releasing vehicles for biomedical applications, J. Mater. Chem. 20(9) (2010) 1624–1637.

[5]. Yang Y, Qi P, Yang Z, Huang NJB, Biotribology, Nitric oxide based strategies for applications of biomedical devices, 1(3) (2015) 177–201.

[6]. Sadrearhami Z, Nguyen TK, Namivandi-Zangeneh R, Jung K, Wong EHH, Boyer C, Recent advances in nitric oxide delivery for antimicrobial applications using polymer-based systems, J Mater Chem B 6(19) (2018) 2945–2959. [PubMed: 32254331]

[7]. Liang H, Nacharaju P, Friedman A, Friedman JM, Nitric oxide generating/releasing materials, Future Sci OA 1(1) (2015).

[8]. Brisbois EJ, Handa H, Major TC, Bartlett RH, Meyerhoff ME, Long-term nitric oxide release and elevated temperature stability with S-nitroso-N-acetylpenicillamine (SNAP)-doped Elast-eon E2As polymer, Biomaterials 34(28) (2013) 6957–66. [PubMed: 23777908]

[9]. Mondal A, Douglass M, Hopkins SP, Singha P, Tran M, Handa H, Brisbois EJ, Multifunctional S-Nitroso-N-acetylpenicillamine-Incorporated Medical-Grade Polymer with Selenium Interface for Biomedical Applications, ACS Appl Mater Interfaces 11(38) (2019) 34652–34662. [PubMed: 31483604]

[10]. Cheng J, He K, Shen Z, Zhang G, Yu Y, Hu J, Nitric Oxide (NO)-Releasing Macromolecules: Rational Design and Biomedical Applications, Front Chem 7 (2019) 530. [PubMed: 31403044]

[11]. Eroy-Reveles AA, Mascharak PK, Nitric oxide-donating materials and their potential in pharmacological applications for site-specific nitric oxide delivery, Future Med Chem 1(8) (2009) 1497–507. [PubMed: 21426062]

[12]. Pant J, Pedaparthi S, Hopkins SP, Goudie MJ, Douglass ME, Handa H, Antibacterial and Cellular Response Toward a Gasotransmitter-Based Hybrid Wound Dressing, ACS Biomaterials Science & Engineering 5(8) (2019) 4002–4012. [PubMed: 33443422]

[13]. Goudie MJ, Pant J, Handa H, Liquid-infused nitric oxide-releasing (LINORel) silicone for decreased fouling, thrombosis, and infection of medical devices, Sci Rep 7(1) (2017) 13623. [PubMed: 29051609]

[14]. Douglass ME, Goudie MJ, Pant J, Singha P, Hopkins S, Devine R, Schmiedt CW, Handa HJAABM, Catalyzed Nitric Oxide Release via Cu Nanoparticles Leads to an Increase in Antimicrobial Effects and Hemocompatibility for Short-Term Extracorporeal Circulation, 2(6) (2019) 2539–2548.

[15]. Hopkins SP, Frost MC, Synthesis and Characterization of Controlled Nitric Oxide Release from S-Nitroso-N-Acetyl-d-Penicillamine Covalently Linked to Polyvinyl Chloride (SNAP-PVC), Bioengineering (Basel) 5(3) (2018) 72.

[16]. Frost MC, Meyerhoff ME, Controlled photoinitiated release of nitric oxide from polymer films containing S-nitroso-N-acetyl-DL-penicillamine derivatized fumed silica filler, J Am Chem Soc 126(5) (2004) 1348–9. [PubMed: 14759186]

[17]. Hopkins SP, Pant J, Goudie MJ, Schmiedt C, Handa H, Achieving Long-Term Biocompatible Silicone via Covalently Immobilized S-Nitroso- N-acetylpenicillamine (SNAP) That Exhibits 4 Months of Sustained Nitric Oxide Release, ACS Appl Mater Interfaces 10(32) (2018) 27316–27325. [PubMed: 30028941]

[18]. VanWagner M, Rhadigan J, Lancina M, Lebovsky A, Romanowicz G, Holmes H, Brunette MA, Snyder KL, Bostwick M, Lee BP, Frost MC, Rajachar RM, S-nitroso-N-acetylpenicillamine (SNAP) derivatization of peptide primary amines to create inducible nitric oxide donor biomaterials, ACS Appl Mater Interfaces 5(17) (2013) 8430–9. [PubMed: 23964741]

[19]. King SB, Mechanisms and novel directions in the biological applications of nitric oxide donors, Free Radic Biol Med 37(6) (2004) 735–6. [PubMed: 15304248]

[20]. Soto RJ, Yang L, Schoenfisch MH, Functionalized Mesoporous Silica via an Aminosilane Surfactant Ion Exchange Reaction: Controlled Scaffold Design and Nitric Oxide Release, ACS Appl Mater Interfaces 8(3) (2016) 2220–31. [PubMed: 26717238]

[21]. Shin JH, Metzger SK, Schoenfisch MH, Synthesis of nitric oxide-releasing silica nanoparticles, J Am Chem Soc 129(15) (2007) 4612–9. [PubMed: 17375919]

[22]. Frost MC, Meyerhoff ME, Synthesis, characterization, and controlled nitric oxide release from S-nitrosothiol-derivatized fumed silica polymer filler particles, J Biomed Mater Res A 72(4) (2005) 409–19. [PubMed: 15682428]

[23]. Zhang H, Annich GM, Miskulin J, Stankiewicz K, Osterholzer K, Merz SI, Bartlett RH, Meyerhoff ME, Nitric oxide-releasing fumed silica particles: synthesis, characterization, and biomedical application, J Am Chem Soc 125(17) (2003) 5015–24. [PubMed: 12708851]

[24]. Grommersch BM, Pant J, Hopkins SP, Goudie MJ, Handa H, Biotemplated Synthesis and Characterization of Mesoporous Nitric Oxide-Releasing Diatomaceous Earth Silica Particles, ACS Appl Mater Interfaces 10(3) (2018) 2291–2301. [PubMed: 29278482]

[25]. Shchukin DG, Sukhorukov GB, Price RR, Lvov YM, Halloysite nanotubes as biomimetic nanoreactors, Small 1(5) (2005) 510–3. [PubMed: 17193477]

[26]. Liu M, Jia Z, Jia D, Zhou C, Recent advance in research on halloysite nanotubes-polymer nanocomposite, Progress in Polymer Science 39(8) (2014) 1498–1525.

[27]. Kamble R, Ghag M, Gaikawad S, Panda B.K.J.J.o.a.s.r., Halloysite Nanotubes and Applications: A Review, 3(2) (2012).

[28]. Kadam AA, Jang J, Lee DS, Supermagnetically Tuned Halloysite Nanotubes Functionalized with Aminosilane for Covalent Laccase Immobilization, ACS Appl Mater Interfaces 9(18) (2017) 15492–15501. [PubMed: 28418639]

[29]. Tan D, Yuan P, Annabi-Bergaya F, Yu H, Liu D, Liu H, He H, Natural halloysite nanotubes as mesoporous carriers for the loading of ibuprofen, Microporous and Mesoporous Materials 179 (2013) 89–98.

[30]. Lvov Y, Aerov A, Fakhrullin R, Clay nanotube encapsulation for functional biocomposites, Adv Colloid Interface Sci 207 (2014) 189–98. [PubMed: 24268974]

[31]. Lazzara G, Cavallaro G, Panchal A, Fakhrullin R, Stavitskaya A, Vinokurov V, Lvov Y, An assembly of organic-inorganic composites using halloysite clay nanotubes, Current Opinion in Colloid & Interface Science 35 (2018) 42–50.

[32]. Hanif M, Jabbar F, Sharif S, Abbas G, Farooq A, Aziz M, Halloysite nanotubes as a new drug-delivery system: a review, Clay Minerals 51(3) (2018) 469–477.

[33]. Hu Y, Chen J, Li X, Sun Y, Huang S, Li Y, Liu H, Xu J, Zhong S, Multifunctional halloysite nanotubes for targeted delivery and controlled release of doxorubicin in-vitro and in-vivo studies, Nanotechnology 28(37) (2017) 375101. [PubMed: 28767041]

[34]. Liu M, Chang Y, Yang J, You Y, He R, Chen T, Zhou C, Functionalized halloysite nanotube by chitosan grafting for drug delivery of curcumin to achieve enhanced anticancer efficacy, J Mater Chem B 4(13)(2016)2253–2263. [PubMed: 32263221]

[35]. Jiang W-T, Chang P-H, Tsai Y, Li Z, Halloysite nanotubes as a carrier for the uptake of selected pharmaceuticals, Microporous and Mesoporous Materials 220 (2016) 298–307.

[36]. Long Z, Zhang J, Shen Y, Zhou C, Liu M, Polyethyleneimine grafted short halloysite nanotubes for gene delivery, Mater Sci Eng C Mater Biol Appl 81 (2017) 224–235. [PubMed: 28887968]

[37]. Long Z, Wu YP, Gao HY, Li YF, He RR, Liu M, Functionalization of Halloysite Nanotubes via Grafting of Dendrimer for Efficient Intracellular Delivery of siRNA, Bioconjug Chem 29(8) (2018) 2606–2618. [PubMed: 29947505]

[38]. Santos AC, Ferreira C, Veiga F, Ribeiro AJ, Panchal A, Lvov Y, Agarwal A, Halloysite clay nanotubes for life sciences applications: From drug encapsulation to bioscaffold, Adv Colloid Interface Sci 257 (2018) 58–70. [PubMed: 29887382]

[39]. Massaro M, Cavallaro G, Colletti CG, D'Azzo G, Guemelli S, Lazzara G, Pieraccini S, Riela S, Halloysite nanotubes for efficient loading, stabilization and controlled release of insulin, J Colloid Interface Sci 524 (2018) 156–164. [PubMed: 29649624]

[40]. Fix D, Andreeva DV, Lvov YM, Shchukin DG, Möhwald HJAFM, Application of inhibitor-loaded halloysite nanotubes in active anti-corrosive coatings, 19(11) (2009) 1720–1727.

[41]. Zahidah KA, Kakooei S, Ismail MC, Bothi Raja P, Halloysite nanotubes as nanocontainer for smart coating application: A review, Progress in Organic Coatings 111 (2017) 175–185.

[42]. Joshi A, Abdullayev E, Vasiliev A, Volkova O, Lvov Y, Interfacial modification of clay nanotubes for the sustained release of corrosion inhibitors, Langmuir 29(24) (2013) 7439–48. [PubMed: 23214412]

[43]. Shchukin DG, Möhwald HJAFM, Surface-engineered nanocontainers for entrapment of corrosion inhibitors, 17(9) (2007) 1451–1458.

[44]. Abdullayev E, Lvov Y, Clay nanotubes for corrosion inhibitor encapsulation: release control with end stoppers, Journal of Materials Chemistry 20(32) (2010) 6681–6687.

[45]. Shu Z, Zhang Y, Yang Q, Yang H, Halloysite Nanotubes Supported Ag and ZnO Nanoparticles with Synergistically Enhanced Antibacterial Activity, Nanoscale Res Lett 12(1) (2017) 135. [PubMed: 28235369]

[46]. Hendessi S, Sevinis EB, Unal S, Cebeci FC, Menceloglu YZ, Unal H, Antibacterial sustained-release coatings from halloysite nanotubes/waterborne polyurethanes, Progress in Organic Coatings 101 (2016)253–261.

[47]. Patel S, Jammalamadaka U, Sun L, Tappa K, Mills DKJB, Sustained release of antibacterial agents from doped halloysite nanotubes, 3(1) (2016) 1.

[48]. Zhang Y, Chen Y, Zhang H, Zhang B, Liu J, Potent antibacterial activity of a novel silver nanoparticle-halloysite nanotube nanocomposite powder, J Inorg Biochem 118 (2013) 59–64. [PubMed: 23123339]

[49]. Fizir M, Dramou P, Dahiru NS, Ruya W, Huang T, He H, Halloysite nanotubes in analytical sciences and in drug delivery: A review, Mikrochim Acta 185(8) (2018) 389. [PubMed: 30046919]

[50]. Moynihan HA, Roberts SM, Preparation of some novel S-nitroso compounds as potential slow-release agents of nitric oxide in vivo, Journal of the Chemical Society, Perkin Transactions 1 (7) (1994) 797–805.

[51]. Zeng S, Reyes C, Liu J, Rodgers PA, Wentworth SH, Sun L, Facile hydroxylation of halloysite nanotubes for epoxy nanocomposite applications, Polymer 55(25) (2014) 6519–6528.

[52]. Wang F, Zhang X, Ma Y, Yang W, Synthesis of HNTs@PEDOT composites via in situ chemical oxidative polymerization and their application in electrode materials, Applied Surface Science 427 (2018) 1038–1045.

[53]. Pant J, Goudie MJ, Hopkins SP, Brisbois EJ, Handa H, Tunable Nitric Oxide Release from S-Nitroso-N-acetylpenicillamine via Catalytic Copper Nanoparticles for Biomedical Applications, ACS Appl Mater Interfaces 9(18) (2017) 15254–15264. [PubMed: 28409633]

[54]. Ghalei S, Asadi H, Ghalei B.J.J.o.A.P.S., Zein nanoparticle-embedded electrospun PVA nanofibers as wound dressing for topical delivery of anti-inflammatory diclofenac, 135(33) (2018) 46643.

[55]. Saraji M, Jafari MT, Mossaddegh M.J.A.c.a., Chemically modified halloysite nanotubes as a solid–phase microextraction coating, 964 (2017) 85–95.

[56]. Riza Erdogan A, Kaygusuz I, Kaynak C.J.P.c., Influences of aminosilanization of halloysite nanotubes on the mechanical properties of polyamide-6 nanocomposites, 35(7) (2014) 1350–1361.

[57]. Li C, Liu J, Qu X, Guo B, Yang Z.J.J.o.a.p.s., Polymer-modified halloysite composite nanotubes, 110(6) (2008) 3638–3646.

[58]. Kurczewska J, Pecyna P, Ratajczak M, Gajecka M, Schroeder G, Halloysite nanotubes as carriers of vancomycin in alginate-based wound dressing, Saudi Pharm J 25(6) (2017) 911–920. [PubMed: 28951678]

[59]. Lin C-F, Tseng W-T, Feng MS, Formation and characteristics of silicon nanocrystals in plasma-enhanced chemical-vapor-deposited silicon-rich oxide, Journal of Applied Physics 87(6) (2000) 2808–2815.

[60]. Yuan P, Southon PD, Liu Z, Green ME, Hook JM, Antill SJ, Kepert C.J.J.T.J.o.P.C.C., Functionalization of halloysite clay nanotubes by grafting with γ-aminopropyltriethoxysilane, 112(40) (2008) 15742–15751.

[61]. Sun Y, Kunc F, Balhara V, Coleman B, Kodra O, Raza M, Chen M, Brinkmann A, Lopinski GP, Johnston LJ, Quantification of amine functional groups on silica nanoparticles: a multi-method approach, Nanoscale Advances 1(4) (2019) 1598–1607.

[62]. McCarthy CW, Goldman J, Frost MC, Synthesis and Characterization of the Novel Nitric Oxide (NO) Donating Compound, S-nitroso-N-acetyl-D-penicillamine Derivatized Cyclam (SNAP-Cyclam), ACS Appl Mater Interfaces 8(9) (2016) 5898–905. [PubMed: 26859235]

[63]. Xia Z, Baird L, Zimmerman N, Yeager M, Heavy metal ion removal by thiol functionalized aluminum oxide hydroxide nanowhiskers, Applied Surface Science 416 (2017) 565–573.

[64]. Riccio DA, Nugent JL, Schoenfisch MH, Stober Synthesis of Nitric Oxide-Releasing S-Nitrosothiol-Modified Silica Particles, Chem Mater 23(7) (2011) 1727–1735. [PubMed: 21499510]

[65]. Riccio DA, Dobmeier KP, Hetrick EM, Privett BJ, Paul HS, Schoenfisch MH, Nitric oxide-releasing S-nitrosothiol-modified xerogels, Biomaterials 30(27) (2009) 4494–502. [PubMed: 19501904]

[66]. Das A, Mukherjee P, Singla SK, Guturu P, Frost MC, Mukhopadhyay D, Shah VH, Patra CR, Fabrication and characterization of an inorganic gold and silica nanoparticle mediated drug delivery system for nitric oxide, Nanotechnology 21(30) (2010) 305102. [PubMed: 20610873]

[67]. Lautner G, Stringer B, Brisbois EJ, Meyerhoff ME, Schwendeman SP, Controlled light-induced gas phase nitric oxide release from S-nitrosothiol-doped silicone rubber films, Nitric Oxide 86 (2019) 31–37. [PubMed: 30735785]

[68]. Ding X, Wang H, Chen W, Liu J, Zhang Y, Preparation and antibacterial activity of copper nanoparticle/halloysite nanotube nanocomposites via reverse atom transfer radical polymerization, RSC Adv. 4(79) (2014) 41993–41996.

[69]. Duan L, Zhao Q, Liu J, Zhang Y, Antibacterial behavior of halloysite nanotubes decorated with copper nanoparticles in a novel mixed matrix membrane for water purification, Environmental Science: Water Research & Technology 1(6) (2015) 874–881.

[70]. Chen Y, Zhang Y, Liu J, Zhang H, Wang K, Preparation and antibacterial property of polyethersulfone ultrafiltration hybrid membrane containing halloysite nanotubes loaded with copper ions, Chemical Engineering Journal 210 (2012) 298–308.

[71]. Massoumi H, Nourmohammadi J, Marvi MS, Moztarzadeh F, Comparative study of the properties of sericin-gelatin nanofibrous wound dressing containing halloysite nanotubes loaded with zinc and copper ions, International Journal of Polymeric Materials and Polymeric Biomaterials 68(18) (2018) 1142–1153.

[72]. Zhang Y, Jiang J, Liang Q, Zhang B.J.J.o.a.p.s., Modification of halloysite nanotubes with poly (styrene–-butyl acrylate–acrylic acid) via in situ soap-free graft polymerization, 117(5) (2010) 3054–3059.

[73]. Stöber W, Fink A, Bohn E.J.J.o.c., i. science, Controlled growth of monodisperse silica spheres in the micron size range, 26(1) (1968) 62–69.

[74]. Wu Y, Zhang Y, Ju J, Yan H, Huang X, Tan YJP, Advances in Halloysite Nanotubes–Polysaccharide Nanocomposite Preparation and Applications, 11(6) (2019) 987.

[75]. Yuan P, Tan D, Annabi-Bergaya F, Properties and applications of halloysite nanotubes: recent research advances and future prospects, Applied Clay Science 112-113 (2015) 75–93.

[76]. Kuttner C, Tebbe M, Schlaad H, Burgert I, Fery A.J.A.a.m., interfaces, Photochemical Synthesis of Polymeric Fiber Coatings and Their Embedding in Matrix Material: Morphology and Nanomechanical Properties at the Fiber–Matrix Interface, 4(7) (2012) 3484–3492.

[77]. Karaman DS, Manner S, Fallarero A, Rosenholm JMJAA, Current approaches for exploration of nanoparticles as antibacterial agents, (2017) 61.

[78]. Asadi H, Ghaee A, Nourmohammadi J, Mashak A, Electrospun zein/graphene oxide nanosheet composite nanofibers with controlled drug release as antibacterial wound dressing, International Journal of Polymeric Materials and Polymeric Biomaterials 69(3) (2019) 173–185.

[79]. Rimondini L, Fini M, Giardino R, The microbial infection of biomaterials: A challenge for clinicians and researchers. A short review, Journal of applied biomaterials & biomechanics : JABB 3(1) (2005) 1–10. [PubMed: 20799234]

[80]. Percival SL, Bowler PG, Russell D, Bacterial resistance to silver in wound care, J Hosp Infect 60(1) (2005) 1–7. [PubMed: 15823649]

[81]. Chambers HF, Deleo FR, Waves of resistance: Staphylococcus aureus in the antibiotic era, Nat Rev Microbiol 7(9) (2009) 629–41. [PubMed: 19680247]

[82]. Schairer DO, Chouake JS, Nosanchuk JD, Friedman AJ, The potential of nitric oxide releasing therapies as antimicrobial agents, Virulence 3(3) (2012) 271–9. [PubMed: 22546899]

[83]. Yang L, Feura ES, Ahonen MJR, Schoenfisch M.H.J.A.h.m., Nitric oxide–releasing macromolecular scaffolds for antibacterial applications, 7(13) (2018) 1800155.

[84]. Howlin RP, Cathie K, Hall-Stoodley L, Cornelius V, Duignan C, Allan RN, Fernandez BO, Barraud N, Bruce KD, Jefferies J, Kelso M, Kjelleberg S, Rice SA, Rogers GB, Pink S, Smith C, Sukhtankar PS, Salib R, Legg J, Carroll M, Daniels T, Feelisch M, Stoodley P, Clarke SC, Connett G, Faust SN, Webb JS, Low-Dose Nitric Oxide as Targeted Anti-biofilm Adjunctive Therapy to Treat Chronic Pseudomonas aeruginosa Infection in Cystic Fibrosis, Mol Ther 25(9) (2017) 2104–2116. [PubMed: 28750737]

[85]. Hasanzadeh Kafshgari M, Delalat B, Harding FJ, Cavallaro A, Makila E, Salonen J, Vasilev K, Voelcker NH, Antibacterial properties of nitric oxide-releasing porous silicon nanoparticles, J Mater Chem B 4(11) (2016) 2051–2058. [PubMed: 32263082]

[86]. Nichols SP, Schoenfisch MH, Nitric oxide-flux dependent bacterial adhesion and viability at fibrinogen-coated surfaces, Biomater Sci 1(11) (2013) 1151–1159.

[87]. Krischel V, Bruch-Gerharz D, Suschek C, Kroncke KD, Ruzicka T, Kolb-Bachofen V, Biphasic effect of exogenous nitric oxide on proliferation and differentiation in skin derived keratinocytes but not fibroblasts, The Journal of investigative dermatology 111(2) (1998) 286–91. [PubMed: 9699731]

[88]. Gansauge S, Gansauge F, Nussler AK, Rau B, Poch B, Schoenberg MH, Beger HG, Exogenous, but not endogenous, nitric oxide increases proliferation rates in senescent human fibroblasts, FEBS letters 410(2–3) (1997) 160–4. [PubMed: 9237621]

[89]. Du M, Islam MM, Lin L, Ohmura Y, Moriyama Y, Fujimura S, Promotion of proliferation of murine BALB/C3T3 fibroblasts mediated by nitric oxide at lower concentrations, Biochemistry and molecular biology international 41(3) (1997) 625–31. [PubMed: 9090471]

[90]. Ghalei S, Mondal A, Hopkins S, Singha P, Devine R, Handa H, Silk Nanoparticles: A Natural Polymeric Platform for Nitric Oxide Delivery in Biomedical Applications, ACS Appl Mater Interfaces (2020).

[91]. Nurhasni H, Cao J, Choi M, Kim I, Lee BL, Jung Y, Yoo JW, Nitric oxide-releasing poly(lactic-co-glycolic acid)-polyethylenimine nanoparticles for prolonged nitric oxide release, antibacterial efficacy, and in vivo wound healing activity, International journal of nanomedicine 10 (2015) 3065–80. [PubMed: 25960648]

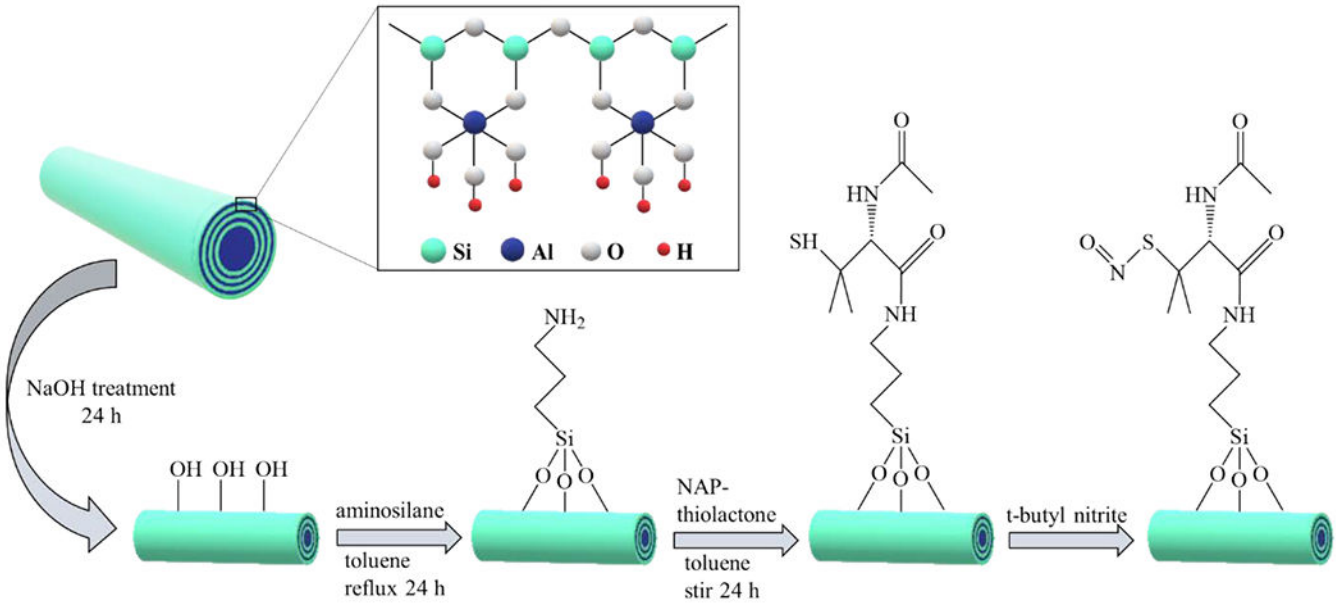

Figure 1.
Schematic representing the chemical synthesis of NO-releasing halloysite nanotubes

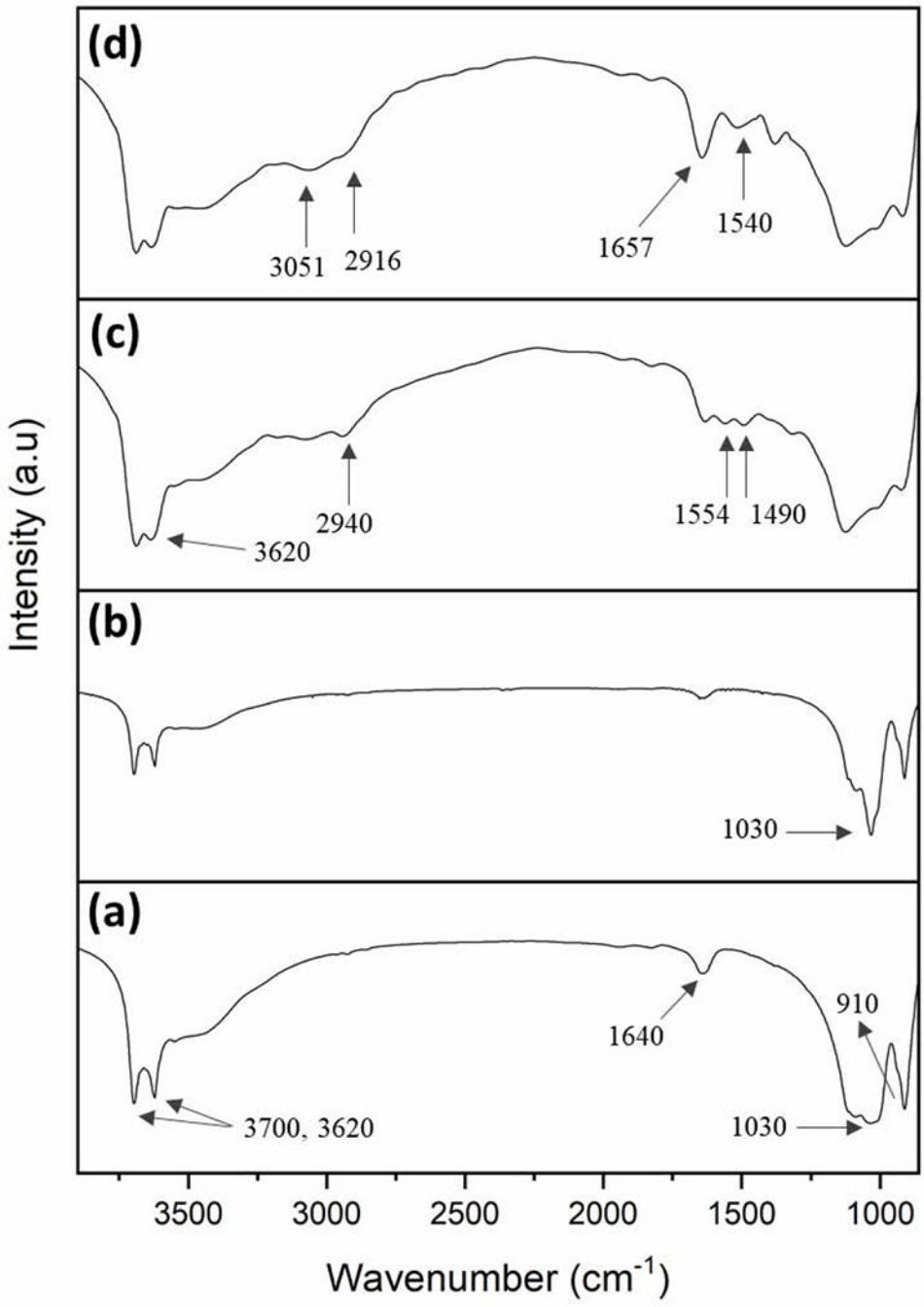

Figure 2.
FTIR spectra of a) unmodified HNT, b) HNT-OH, c) HNT-APTMS, and d) HNT-NAP

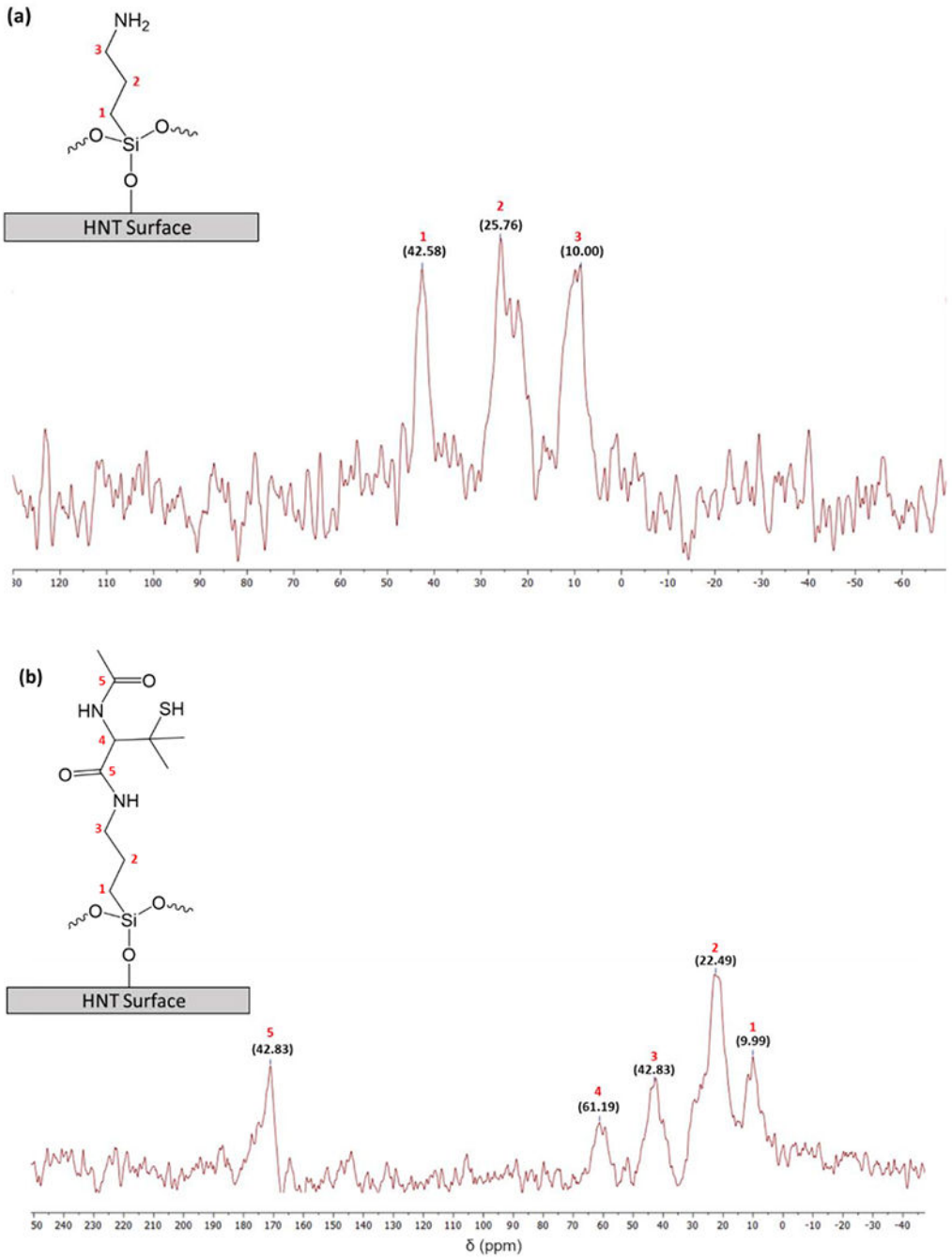

Figure 3.

^{13}C CP/MAS NMR spectra of (a) APTMS modified HNTs and (b) NAP modified HNTs. The APTMS carbon peaks have been thoroughly investigated in previous literature [60]. While most of the carbon peaks in the NAP functionalized HNTs are overlapped in the methyl region (between 20–50 ppm), there is a distinct carbonyl peak at 171 ppm indicating successful NAP attachment.

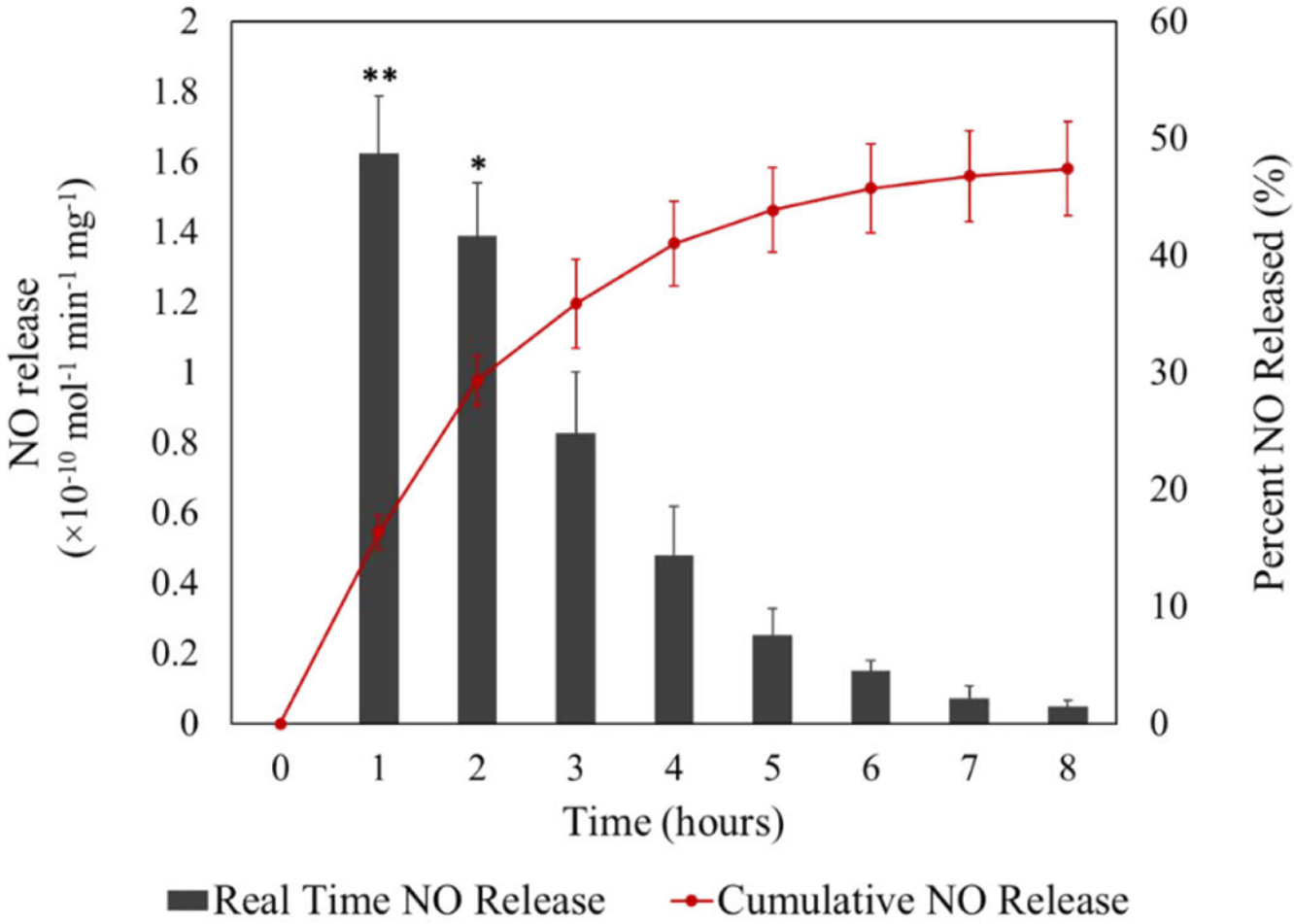

Figure 4.

Cumulative and real-time NO release from HNT-SNAP soaking in PBS buffer at 37 °C in the dark. The red graph (cumulative NO release) and the black bar graph (real-time NO release) correspond to the right and left axes, respectively. Data represent the mean ± SD (n=4). *p*-values ≤ 0.05 and ≤ 0.01 are shown with * and **, respectively.

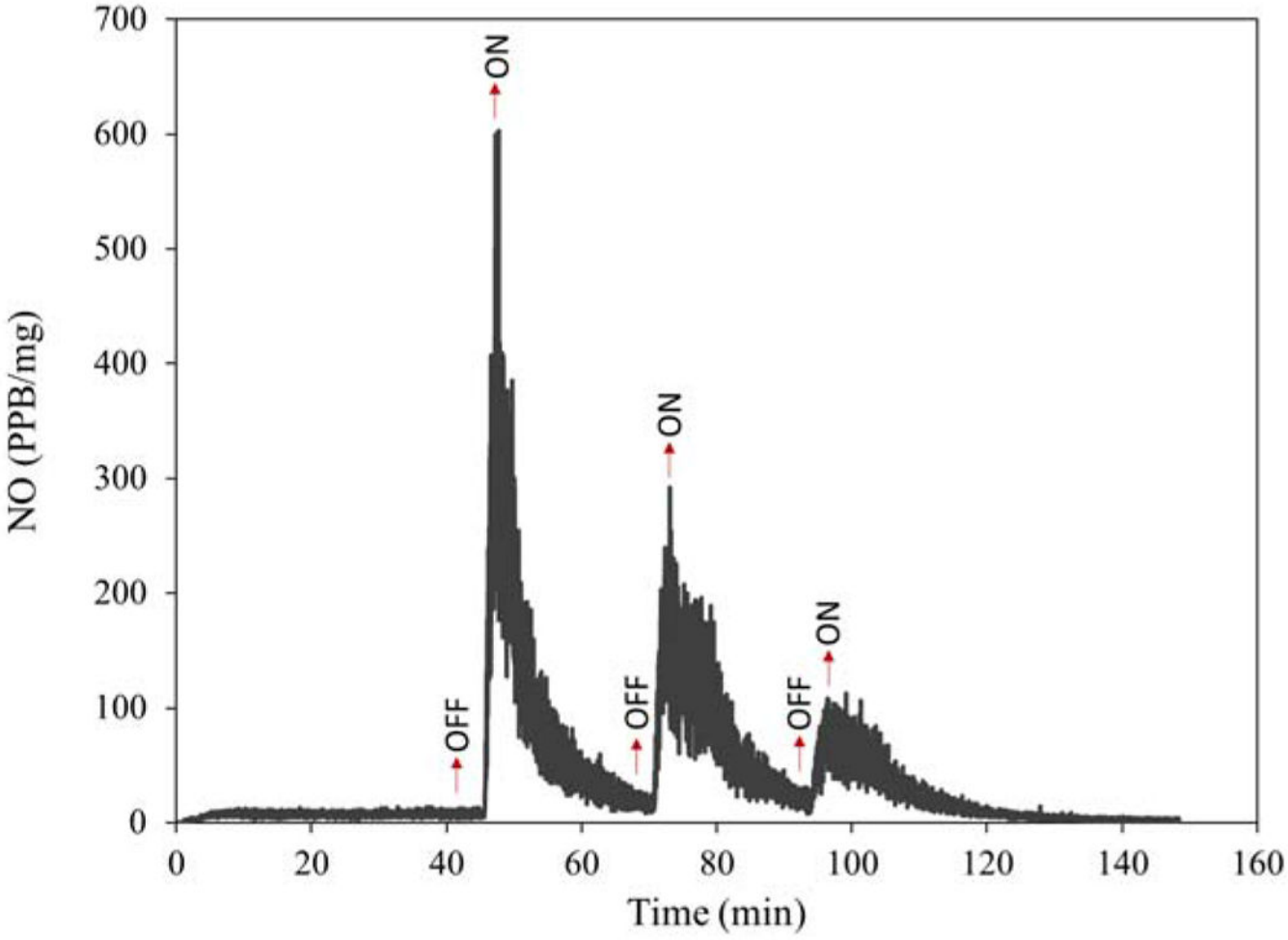

Figure 5.
Real-time NO release from HNT-SNAP under light irradiation.

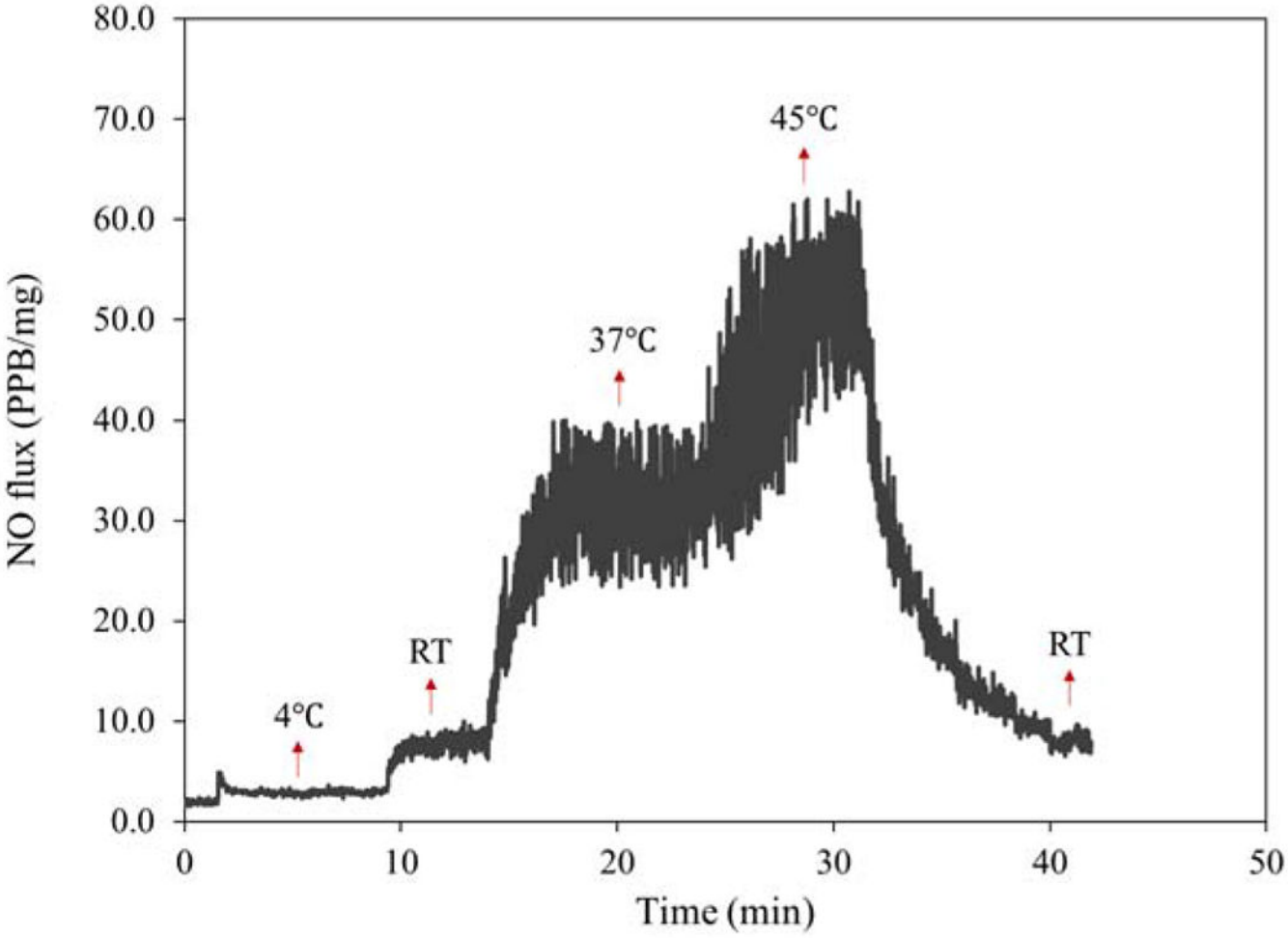

Figure 6.
Real-time NO release from HNT-SNAP under different temperatures.

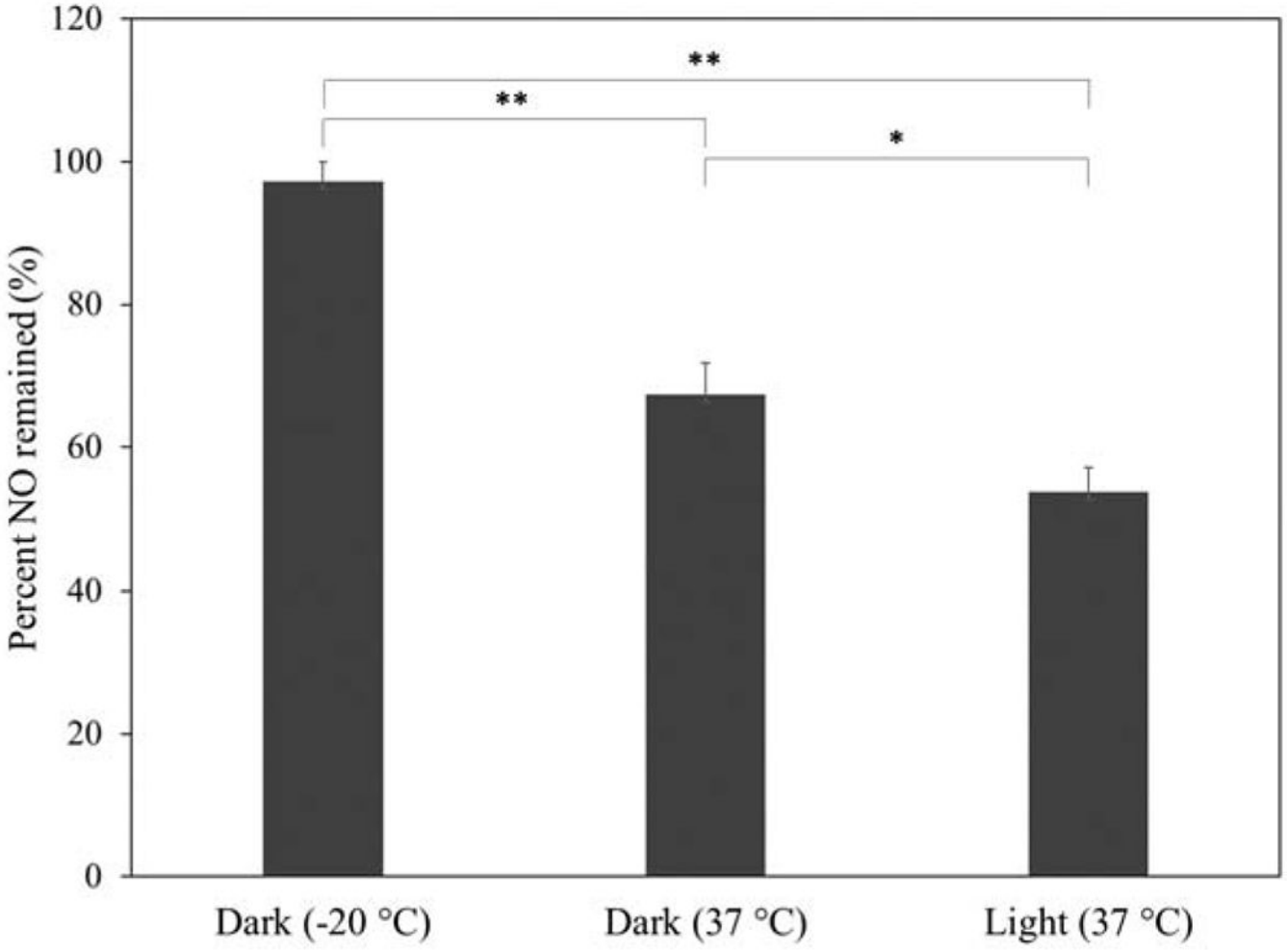

Figure 7.
Storage stability of HNT-SNAP at different conditions over 4 weeks.

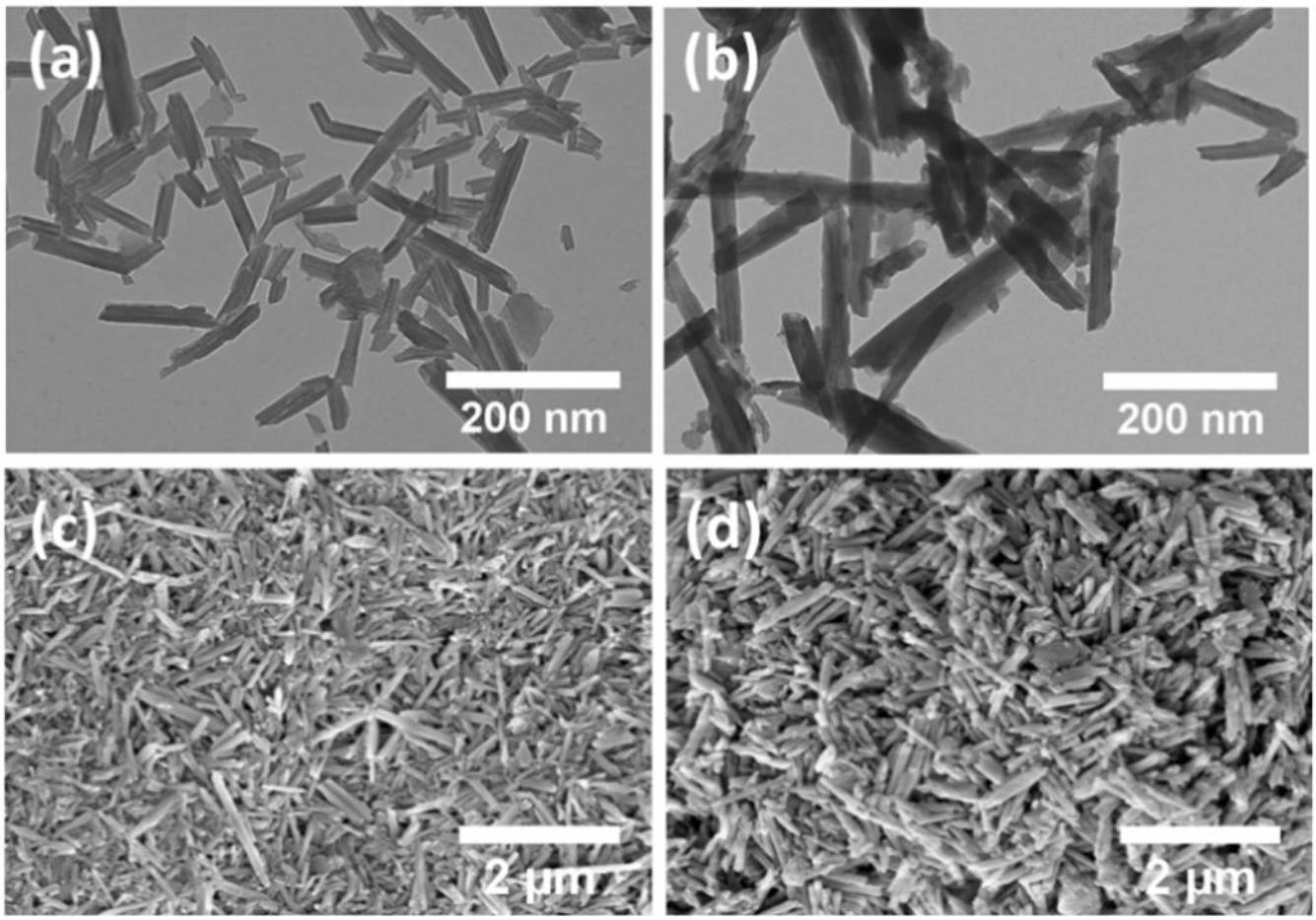

Figure 8.
TEM images (a,b) and SEM images (c,d) of HNTs (a,c,) and HNT-SNAP (b,d).

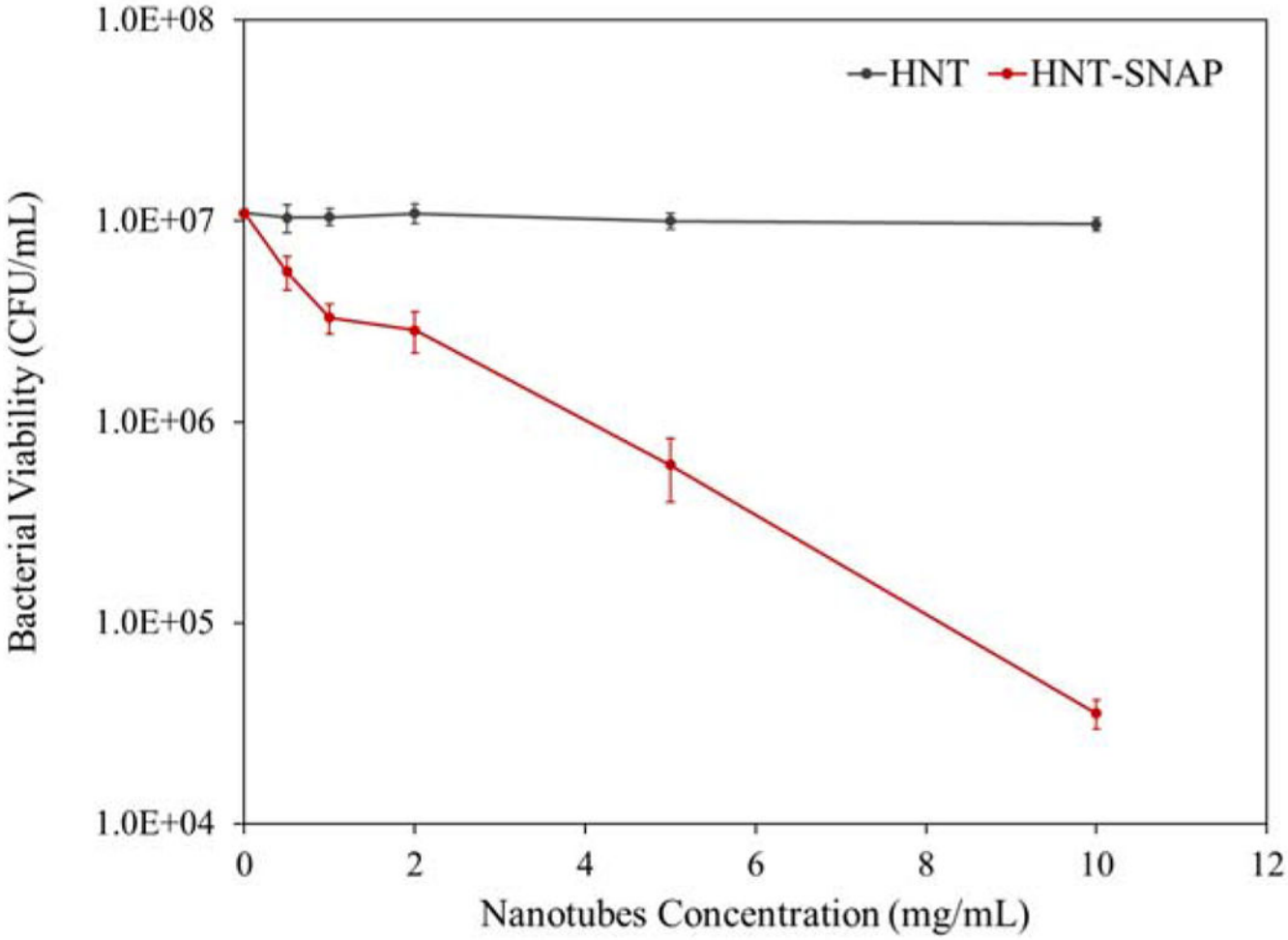

Figure 9.
Antibacterial activity of HNT and HNT-SNAP against *S. aureus* after 24 h (n=5)

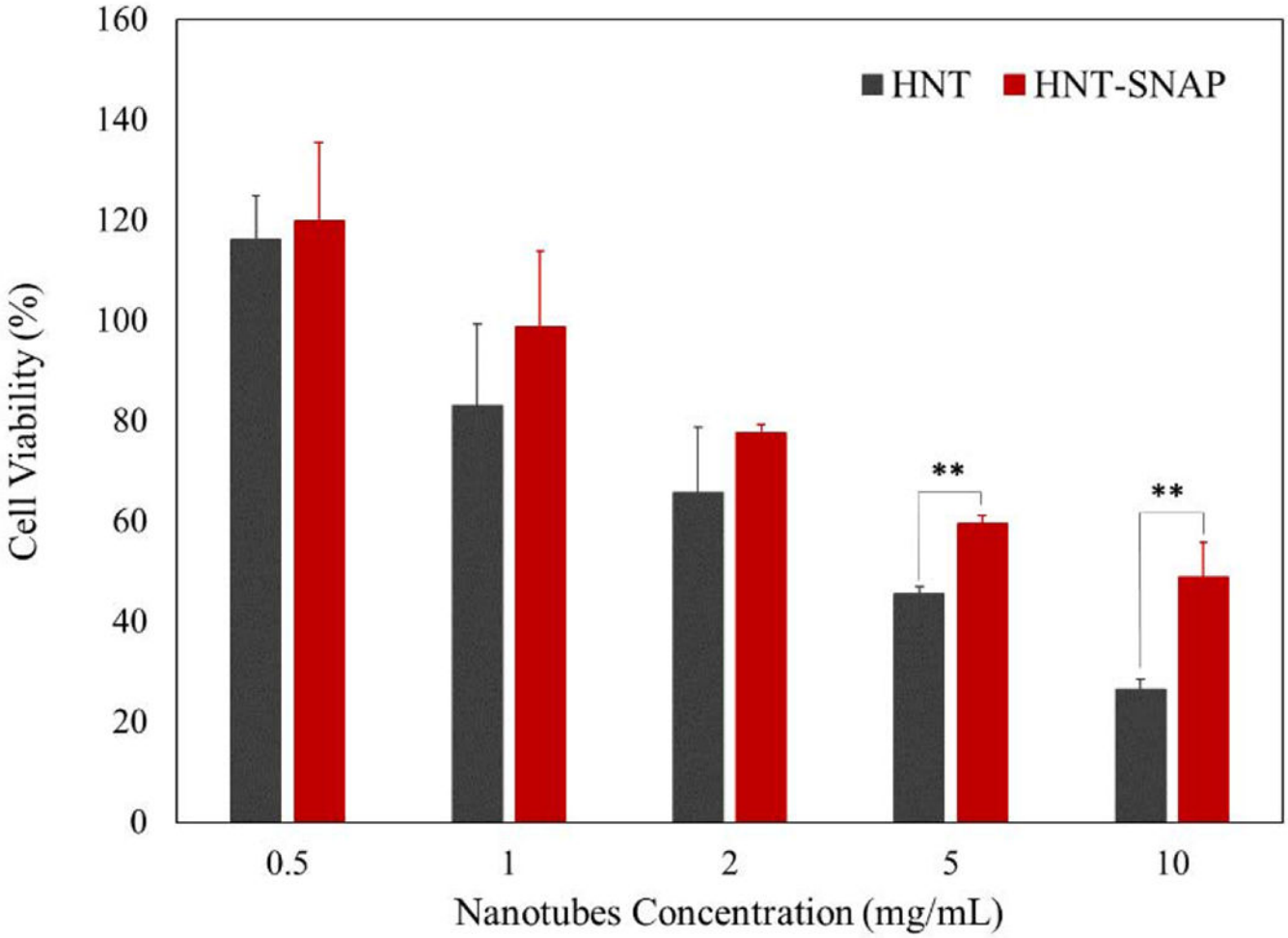

Figure 10.

24 h viability of 3T3 mouse fibroblast cells (as a percentage relative to control) using WST dye-based CCK-8 assay. The error bar represents the SD (n=6). *p*-values ≤ 0.01 are shown with **.

Table 1.

Amine Content, thiol Content, conversion ratio, total NO loading, and nitrosation efficiency of modified HNTs (n=4)

Amine content (μmol/mg)	Thiol content (μmol/mg)	Conv. ratio (%)	Total NO (μmol/mg)	Nitrosation efficiency (%)
0.252 ± 0.009	0.202 ± 0.015	80.15	0.100 ± 0.07	49.50

Table 2.

Viability reduction efficiency values of *S. aureus* bacterial strain after exposure to different concentrations of HNT-SNAP for 24 h (n=5).

HNT-SNAP concentration (mg/mL)	*S. aureus* reduction efficiency (%)
0.5	48.9 ± 3.9 **
1	69.9 ± 9.8 **
2	73.8 ± 5.0 **
5	94.4 ± 1.9 **
10	99.6 ± 0.1 **

** indicates *P*-values ≤ 0.01 versus HNTs at the same concentration

Table 3.

Viability values of 3T3 mouse fibroblast cells after direct exposure to different concentrations of HNT and HNT-SNAP for 24 h.

Nanotubes concentration (mg/mL)	Cell viability (%)	
	HNT	HNT-SNAP
0.5	116.2 ± 8.7	119.8 ± 15.6
1	83.1 ± 16.2	98.8 ± 15.0
2	65.8 ± 13.0	77.6 ± 1.6
5	45.5 ± 1.5	59.4 ± 1.6**
10	26.4 ± 2.1	48.8 ± 7.0**

** indicates *P*-values ≤0.01 obtained by comparison of HNT-SNAP and HNT at the same concentration